Matheus Pereira Porto

Theoretical and experimental studies on boiling heat transfer for the zeotropic mixture R-407C

Belo Horizonte, Brazil

2013

Matheus Pereira Porto

Theoretical and experimental studies on boiling heat transfer for the zeotropic mixture R-407C

Submitted in partial fulfillment of the requirements for the degree of Doctorate in Mechanical Engineering in the Programa de Pós Graduação em Engenharia Mecânica da Universidade Federal de Minas Gerais at Belo Horizonte, 2013.

Universidade Federal de Minas Gerais – UFMG

Escola de Engenharia da UFMG

Programa de Pós-Graduação em Engenharia Mecânica da UFMG

Advisor: Luiz Machado

Co-advisor: Carlos F. M. Coimbra

Belo Horizonte, Brazil

2013

Matheus Pereira Porto
Theoretical and experimental studies on boiling heat transfer for the zeotropic mixture R-407C/ Matheus Pereira Porto. – Belo Horizonte, Brazil, 2013-
83 p. : il. (algumas color.) ; 30 cm.

Advisor: Luiz Machado

Doctoral Thesis – Universidade Federal de Minas Gerais – UFMG
Escola de Engenharia da UFMG
Programa de Pós-Graduação em Engenharia Mecânica da UFMG, 2013.

1. Heat transfer coefficient. 2. zeotropic mixtures. I. Machado, L. II. UFMG. III. PPGMEC.

Matheus Pereira Porto

Theoretical and experimental studies on boiling heat transfer for the zeotropic mixture R-407C

Submitted in partial fulfillment of the requirements for the degree of Doctorate in Mechanical Engineering in the Programa de Pós Graduação em Engenharia Mecânica da Universidade Federal de Minas Gerais at Belo Horizonte, 2013.

Approved in Belo Horizonte, Brazil, september 13, 2013:

Luiz Machado
Advisor - PPGMEC

Carlos F. M. Coimbra
Co-advisor - UCSD

Ricardo Nicolau Nassar Koury
Professor - PPGMEC

Antônio Augusto Torres Maia
Professor - PPGMEC

Carlos Umberto da Silva Lima
Professor - UFPA

Antônio Carlos Lopes da Costa
Researcher - CDTN

Belo Horizonte, Brazil
2013

Abstract

This work concerns theorical and experimental methods for understanding the heat transfer mechanisms for a zeotropic fluid, namely R-407C. The refrigerant R-407C is a mixture of three refrigerants, R-134a, R-32, and R-125, which may replace R-22 in future refrigerant systems. Due to the degradation of heat transfer coefficients in mixtures such as R-407C, the classical relations may overestimate the experimental heat transfer rates. A correction based on nucleate boiling suppression factors that corrects a previously proposed relation is used to minimize the degradation error. The newly proposed relation was developed through a robust methodology based on genetic algorithm (GA) optimization for three additional refrigerants R-404a, R134a and R-22. A discussion about inventory is also presented, where a modified Otaki method is proposed for the more realistic scenario that corresponds of not knowing a priori the heat transfer coefficient. The inventory obtained by the modified Otaki method is higher than the one obtained by the traditional Otaki method. Both methods yield accurate results for R-407C.

List of figures

List of tables

List of abbreviations and acronyms

HTC	Heat transfer coefficients
R	Refrigerant
PPGMEC	Programa de Pós Graduação em Engenharia Mecânica da Universidade Federal de Minas Gerais
DEMEC	Departamento de Engenharia Mecânica da Universidade Federal de Minas Gerais
UCSD	University of California, San Diego
UFPA	Universidade Federal do Pará
CDTN	Centro de Desenvolvimento da Energia Nuclear

List of symbols

d	diameter, m
E	voltage, V
g	gravitational acceleration, ms^{-2}
G	mass flux, $kgm^{-2}s^{-1}$
h	heat transfer coefficient (HTC), $Wm^{-2}K^{-1}$
i	enthalpy, $kJkg^{-1}$
k	thermal conductivity, $Wm^{-1}K^{-1}$
$\dot{Q}$	heat transfer rate, W
$\dot{Q}$"	heat flux, Wm^{-2}
s	standard deviation
u	uncertainty
uc	combined uncertainty
U	mass flow or bulk velocity, ms^{-1}
v	degrees of freedom
x	Molar fraction of liquid
y	Molar fraction of vapor
	Greek
β	Mass transfer velocity, ms^{-1}
χ	Martinelli parameter
Γ	current, A
μ	viscosity, Pa.s
ρ	density, kgm^{-3}

σ	surface tension, Nm^{-1}
	Dimensionless numbers
Fr	Froude number, $G^2\rho^{-2}g^{-1}d^{-1}$
Pr	Prandtl number, $\mu c_p K^{-1}$
Re	Reynolds number, $\rho U d/\mu$
We	Weber number, $G^2 d\rho^{-1}\sigma^{-1}$
	Subscripts
ace	heat exchanger: cold water circuit / auxiliary circuit's evaporator, auxiliary circuit side
cb	convective boiling
$crit$	critical properties
cwc	cold water circuit
cwe	heat exchanger: cold water circuit / auxiliary circuit's evaporator, cold water side
eq	equivalent property - linear proportion between saturation properties and quality
l	saturated liquid, x=0
lv	difference between vapor from liquid saturated properties
mp	micropump, primary circuit
nb	nucleate boiling
ph	pre-heater, primary circuit
$pump$	pump, cold water circuit
tp	two-phase flow
ts	test section
tt	liquid / vapor interface
s	saturated

v	saturated vapor, x=1
w	tube wall

Contents

Introduction

Refrigeration systems have been used widely during the past decades, and currently, a special attention has been paid to solve ecological problems caused by refrigerant fluids. Refrigerant fluids as R-22 are now considered under phasing out process, because they are related to ozone layer depletion and global warming. As a consequence of this fact, new refrigerant fluids are retrofitting R-22 systems. One of the most used candidate is the R-407C. R-407C is a mixture comprised of R-134a, R-32 and R-125, which in a given proportion generates an ecological solution. Because it is a mixture singular properties are expected, as temperature change during phase change, so-called glide. A mixture that presents glide is defined as a zeotropic mixture. In this work, it is used the refrigerant fluid R-407C to improve the understanding on the characteristics of zeotropic fluids, applied for vapor compression refrigeration systems.

Many researchers have been studying refrigeration systems with R-407C. Devotta et al (8) have presented an analysis comparing the performance of an air conditioning designed for R-22, retrofitted with R-407C. R-407C had a lower cooling capacity, 2% to 8% with respect to R-22; Coefficient of performance for R-407C is also lower, 8 to 13.5%. Power consumption for the unit with R-407C was higher, 6 to 7%. Discharge pressures for R-407C were 11-13% higher. Pressure dropping was also discussed, being lower for the R-407C in both evaporator and condenser.

Haberschill et al (9) have shown a steady state model of a refrigeration system with R-407C, showing how the circulation composition can change along the refrigeration circuit. According the authors this change is caused by the glide and the vapor-liquid slip ration. The circulating composition model used is based on the Chen and Kruse (10) methodology. Haberschill et al (9) also showed the influence of leakage and filling cycles, observing the composition changes on the system characteristics; evaporation and condensing temperature increases with the numbers of leakage and recharge cycles, as the mass flow rate and cooling capacity. After nine leakages followed by nine fillings, fluid become impoverished in R-32 and R-125, and enriched in R-134a; its composition vary from 23/25/52 to 22.3/24.4/53.3 %. The overall heat transfer coefficient for R-407C is 30 % lower than the one for R-22 (2900 and $4130 W m^{-2} K^{-1}$, respectively), and the authors justify this fact due to the nucleate boiling degradation observed in mixtures.

Passos et al (11) presents experimental results on nucleate and convective boiling for R-407C, with mass velocity in the range 200 to $300 kg\ m^{-}2\ s^{-1}$, at 770 kPa, inside horizontal smooth and microfin tubes, with outside diameters of 7.0 and 12.7 mm, showing that nucleate boiling was predominant to the first and convective boiling to the latter.

Necula et al (12) presented a steady state modeling of a shell-and-tube evaporator using R-407C. The effects of leakage were also studied. A flow pattern map was used to determine the condition inside the heat exchanger.

Wang and Chiang (13) have presented a discussion about heat transfer characteristics using a R-407C / R-22 for a 6.5mm smooth tube. HTC was experimentally determined for a mass flux range of 100 to 400 $kg\,m^{-2}s^{-1}$ and pressure drop in the range of 100 to 700 $kg\,m^{-2}s^{-1}$. At low mass flux was observed a predominance of nucleate boiling, and a further increasing to 400 $kg\,m^{-2}s^{-1}$ resulted in higher contribution of convective boiling. Both pressure drop and HTC for R-407C are considerably lower than those to R-22, according the authors.

Some authors, as Keumnam et al. (14), Jeng et al. (15) and Youbu-Idrissi et al. (16) have emphasized the characteristics of R-407C with lubricant oil. In this work it is used a micropump, and no oil mixture is used in the circuit. Jeng et al. (16) also presented an analysis for the flow pattern map, comparing R-134a, R-22 and R-407C, concluding that R-407C presents a delay for the transitions, which could be the explanation to the HTC degradation observed in this mixture.

In this work Artificial Neural Networks and Genetic Algorithm are used to create a general robust HTC relation for pure fluids; a reduction factor is applied on this relation to take into account the suppression effects for the R-407C. Validations are presented indicating accurate results.

This thesis is divided in the following chapters:

1. Item 1 - Experimental setup
2. Item 2 - Methodology and literature review
3. Item 3 - Results
4. Item 4 - Conclusion

Part I

Experimental Setup

1 Experimental setup

1.1 Test facilities

Different test facilities were studied by Lima (17), and those were presented in three different categories: with oil contamination (18, 19, 20), with no oil contamination (21, 22) and with parallel circuits (independent of having oil contamination or not).

Facilities with oil contamination have the drawback of miscalculating the thermodynamic properties. This type of facility is generally comprised of a single circuit, with compressor, and there is not the possibility of changing neither evaporation nor condensation temperature.

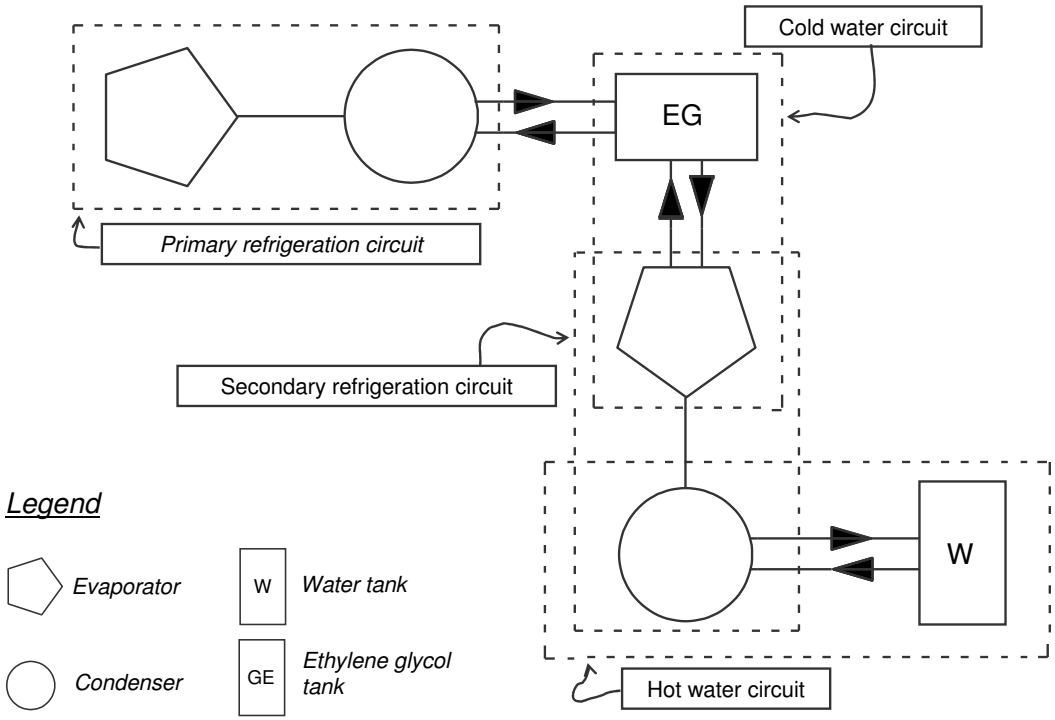

Figure 1 – Schematical of the four parallel circuits experimental facility.

Experimental facilities with no oil contamination are those ones that do not use compressors. It is possible using just gravitational effects to obtain a difference in pressure, but a high difference in level between the evaporator and condenser is required to generate mass flow, which also has the disadvantage of being constant for all experiments.

Experimental facilities with parallel circuits are comprised generally by three or four circuits working at the same time. In case of four, the test section circuit (primary

refrigeration circuit) is in parallel with an ethylene-glycol circuit (cold water circuit), which is cooled by a heat exchanger interlinked to an evaporator located in a conventional refrigeration system (auxiliary refrigeration circuit) to obtain temperature dropping effect; this auxiliary circuit also uses a cooling tower (or an open circuit of water coming from the supply system), used for cooling (or replace) the water that comes from the condenser's heat exchanger (hot water circuit). Figure 2 presents a schematic of the four parallel circuits test facility. In case of using three, the cold water circuit will not be used, and the evaporation temperature will be constant for all experiments.

In this work, it is built a refrigeration test facility with four parallel circuits, to take advantage of working at different evaporation temperatures. A magnetically driven micropump was also used in the primary refrigeration circuit to guarantee no oil contamination during the tests. Also, an inverter was used allowing mass flow rate variation.

1.2 Experimental device

This experimental device is based on the work of Lima (17). Figure 2 presents the experimental facility, highlighting the four parallel circuits, as discussed above. More emphasis will be given to the primary circuit, but more detailed information about the other circuits can be found in Maia (1).

1.2.1 Primary circuit

The primary circuit is comprised of 4 important parts: micropump system, pre-heater, test section and condenser.

The micropump is magnetically driven by a rubber coupling with magnets, connected to an electrical motor, generating the mass flow rate required with no oil contamination; since there is no contact between mechanical parts, lubrication is not required. Figure 3 presents a picture showing the components that comprise the micropump system.

The magnetic coupling was developed inside the laboratory during the facility assemblage, and it is object of a patent, which is being released by the Federal University of Minas Gerais.

As the system uses a pump instead of a compressor, and there are no expansion mechanisms, the difference in pressure realized during the experiments will be just from friction losses.

Pre-heater is responsible for receiving compressed liquid from the pump and delivering two-phase flow fluid to the test section. This component is comprised of an electrical resistance, and its power is controlled by a varistor, varying the voltage output. Different

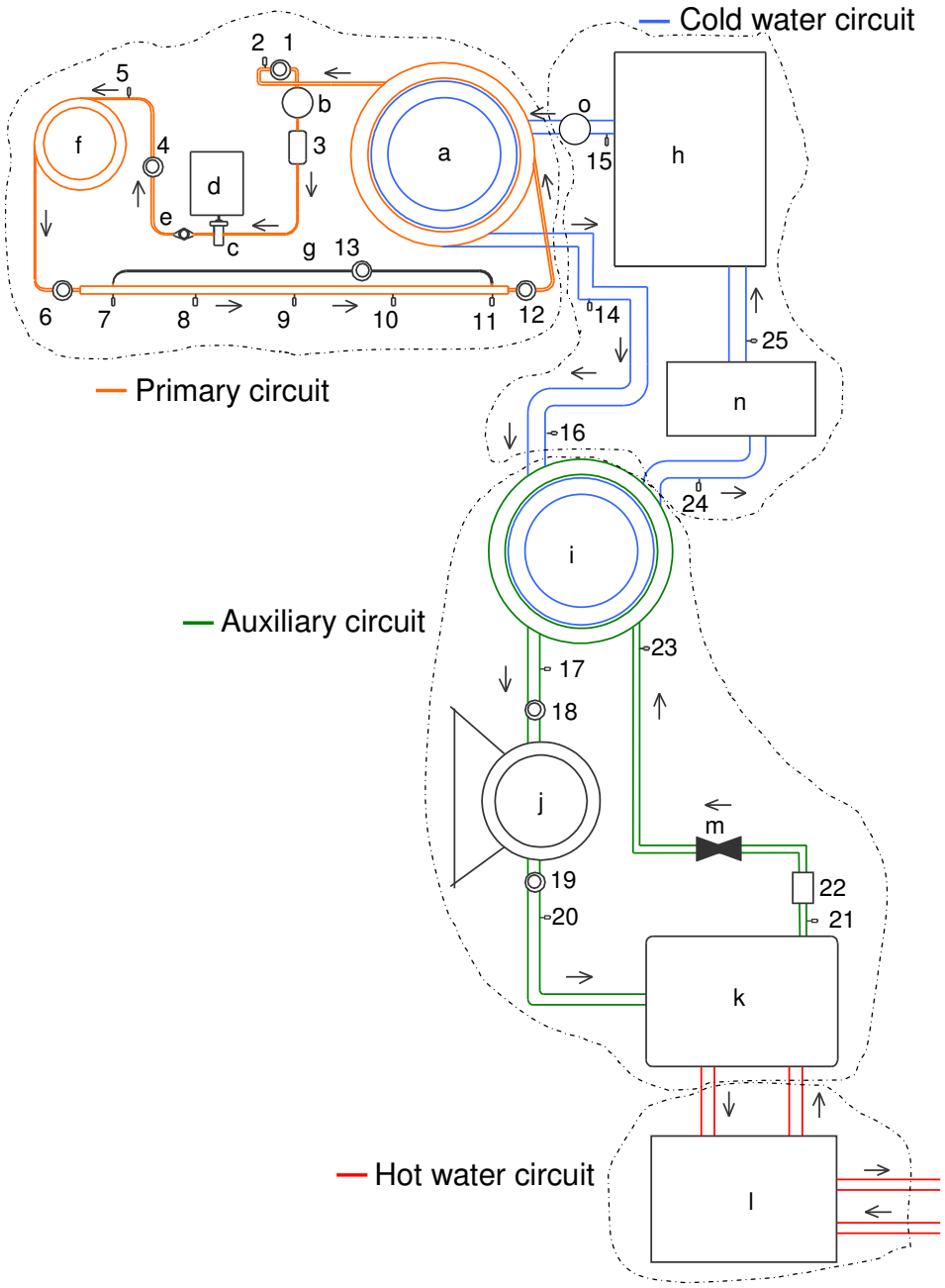

Figure 2 – Schematical of the experimental facility. **In primary circuit**, *letters:* a, condenser; b, liquid bottle; c, micropump; d, electrical motor with inverter; e, butterfly valve; f, pre-heater; g, test section; *numbers:* 1, 4, 6 and 12, absolute pressure transmitters; 13, differential pressure transmitter; 3, Flow meter; 2, 5, 7 - 11, thermocouples. **In cold water circuit**, *letters:* h, ethylene-glycol tank; n, temperature controller; o, pump 2 hp; *numbers:* 14 - 16 and 25, thermocouples. **In auxiliary circuit**, *letters:* i, evaporator; j, compressor with inverter; k, condenser; m, expansion valve; *numbers:* 17, 20, 21, 23, thermocouples; 18, 19, pressure transmitter; 22, mass flow meter. **In hot water circuit**, *letters:* l, water tank.

power output will cause different two phase flow quality. The pre-heater is comprised of a set of 10 resistances with 161 Ω each, arranged in parallel. The equivalent resistance is equal to $(10/161\Omega)^{-}1 = 16.1\ \Omega$. It is not recommended going over 12.5 A, because it is the maximum value allowed by the varistor's manufacturer. Figure 4 shows the Pre-heater and the Varistor during the facility construction.

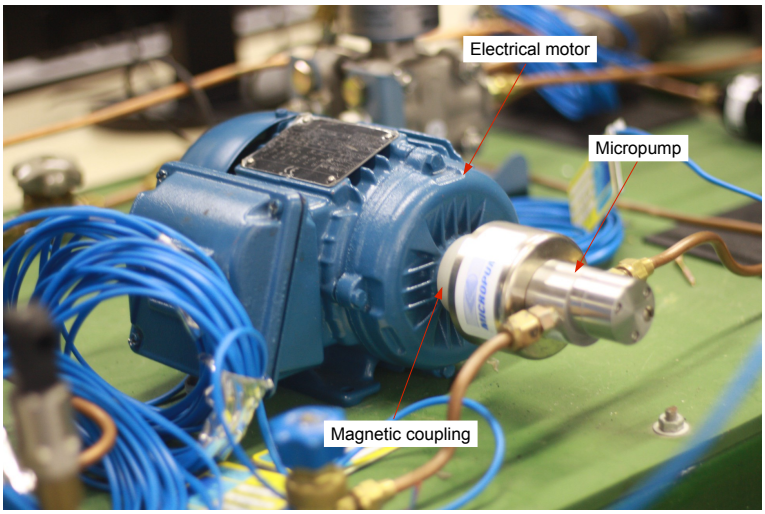

Figure 3 – Motor, coupling and magnetically driven micropump.

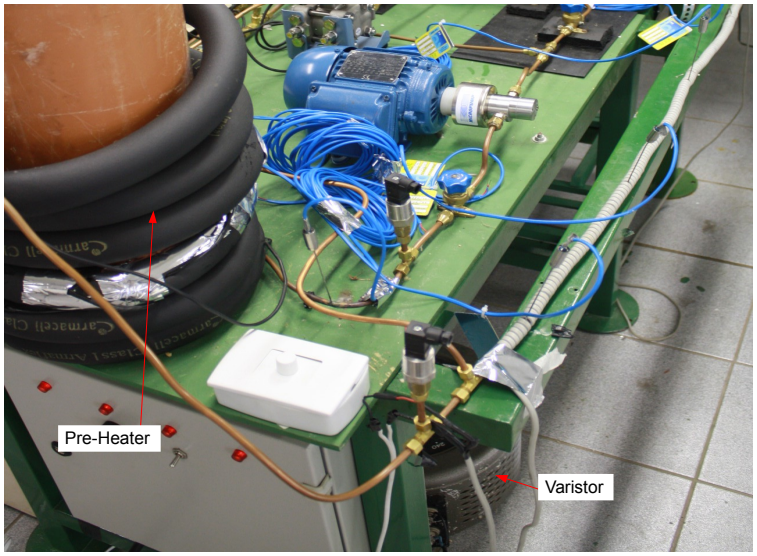

Figure 4 – Pre-heater and varistor.

The test section is the most important part of the experimental device. It is comprised of five thermocouples, two absolute pressure transmitters and one differential pressure transmitter. The tube diameter is 1/4 inch, wrapped around by an electrical resistance with silicon insulation, which is controlled by a variable resistance. Afterward, this test section was covered by a rubber insulation to guarantee an adiabatic condition.

The idea is generating an uniform heat flux on the tube, and after this will be possible determining the heat transfer coefficient (HTC) by using the Newton's law of cooling and the thermal resistance concept (see Fig. 5):

$$h = \frac{\dot{Q}"}{(T_w - T_s)(r_1/r_2)} - \frac{k}{ln(r_2/r_1)\, r_1}, \tag{1.1}$$

and,

$$\dot{Q}'' = \frac{Q}{S} = \frac{Q}{2\pi\, r_2\, L}, \tag{1.2}$$

where h is the HTC ($Wm^{-2}K^{-1}$), Q'' is the heat flux (Wm^{-2}), T_w is the tube internal surface temperature (°C), T_s is the bulk temperature of the fluid (°C), and S is the tube external surface area (m^2), k is the copper tube thermal conductivity. Heat flux is considered one-dimensional and in the radial direction.

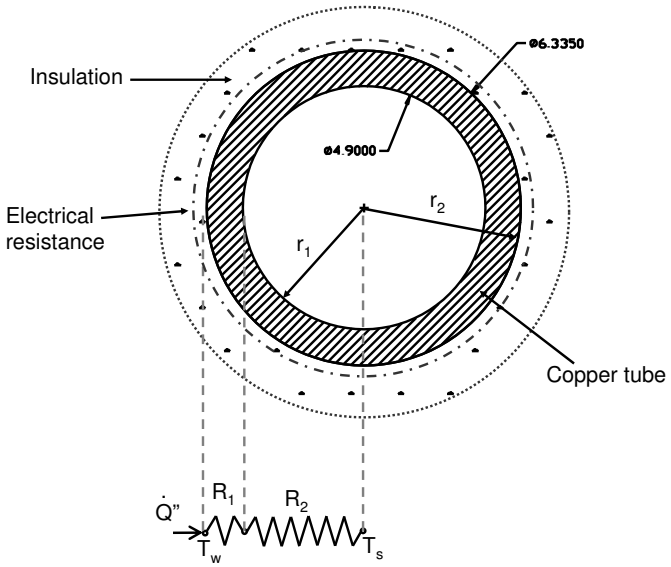

Figure 5 – Determination of the experimental heat transfer coefficient, see Eq. 1.1; where, $R_1 = \frac{1}{2\pi\, r_1\, L\, h}$, and $R_2 = \frac{ln\frac{r_2}{r_1}}{2\pi\, k\, L}$.

The condenser is responsible for cooling the refrigerant, in which was heated by the micropump, pre-heater and test section. The total heat exchange required during this process can be determined using Eq.1.3:

$$\dot{Q}_c = \dot{Q}_{ph} + \dot{Q}_{ts} + \dot{Q}_{mp}, \tag{1.3}$$

where $\dot{Q}_{ph}$, $\dot{Q}_{ts}$ and $\dot{Q}_{mp}$ are the heat transferred by the pre-heater, test section and micropump, respectively, and can be determined as follows:

$$\dot{Q}_{mp} = \dot{W}_{mp} - \dot{V}\Delta P, \tag{1.4}$$

and,

$$\dot{Q}_{ph} = E_{ph}\,\Gamma_{ph}, \tag{1.5}$$

and,

$$\dot{Q}_{ts} = E_{ts}\,\Gamma_{ts}. \tag{1.6}$$

In this work, it is neglected the micropump contribution, due to its low order of magnitude. During an energy balance should be found that all heat transferred by the condenser's heat exchanger (see Fig. 2, letter "a"), in the primary circuit side, it is going to the cold water system.

Particularly during the inventory determination, the geometric properties have to be well-defined to obtain accurate results. Table 1 presents the primary circuit dimensions.

Table 1 – Primary circuit dimensions.

Component	Length	Internal diameter	External diameter
Condenser	19.85 m	7.9 mm	9.5 mm
Low pressure liquid line	1.6 m	4.9 mm	6.35 mm
high pressure liquid line	0.4 m	4.9 mm	6.35 mm
Liquid bottle	0.2 m	0.1 m	-
Pre-heater	2.76 m	4.9 mm	6.35 mm
Test section	1.15 m	4.9 mm	6.35 mm
Vapor line (pre-heater)	0.7 m	4.9 mm	6.35 mm
Vapor line (test section)	0.7 m	4.9 mm	6.35 mm

1.2.2 Cold water circuit

Cold water circuit is comprised of a tank with ethylene-glycol at 30% of composition with 70% of water (see Fig. 2, letter "h"), a 2 hp pump and a PID temperature controller (see letter "n"). Looking at the cold water circuit side, the energy balance among points 14 and 15 shows that:

$$\dot{Q}_c = -\dot{Q}_{pump} + \dot{m}_{cw}\,c_{p,cwc}\,\Delta T_{cwc} = -\dot{Q}_{pump} + \dot{m}_{cw}\,c_{p,cwc}\,(T_{14} - T_{15}), \tag{1.7}$$

where $\dot{Q}_c$, $\dot{Q}_{pump}$, $\dot{m}_{cw}$, $c_{p,cwc}$ and ΔT_{cwc} are the condenser heat transfer rate, cold water mass flow rate, heat transfer capacity for the cold water circuit and temperature differ-

ence for the water, respectively. It is considered $\dot{Q}_{pump}$ negligible since the temperature difference given by this term is lower than the thermocouples uncertainty.

The ethylene-glycol water mass flow rate will be determined indirectly during the experiments, feeding during one minute a recipient, and weighting it using a precision balance, also subtracting the void recipient weight; mass over time spent will give the mass flow rate.

1.2.3 Auxiliary circuit

Auxiliary circuit is a conventional refrigeration system driven by a reciprocating compressor and an expansion mechanism, also using R-134a as refrigerant fluid. Considering a control volume on the evaporator (see Fig. 2, letter "i"), it is possible to obtain the energy balance as:

$$\dot{Q}_{cwe} = \dot{Q}_{ace}, \tag{1.8}$$

and,

$$\dot{m}_{cw}\, c_{p,cwe}\, (T_{24} - T_{16}) = \dot{m}_{ace}\, (i_{17} - i_{16}), \tag{1.9}$$

where, $\dot{Q}_{cwe}$ is the heat transfer rate from the cold water circuit, and $\dot{Q}_{ace}$ is the heat transfer at the R-134a side; $c_{p,cwe}$, T_{24} and T_{16} are the average heat transfer capacity to the points 24 and 16, temperature at the point 24 and at the point 16, respectively; $\dot{m}_{ace}$ is the R-134a mass flow rate (see the mass flow meter in Fig. 2, number 22), i_{16} is the enthalpy at the evaporator's inlet (see number 16) and i_{17} is the enthalpy at outlet (see number 17).

1.2.4 Overall energy balance between primary and auxiliary circuits

The water in the cold water circuit is the matter that conveys the energy from the primary to the auxiliary circuit. The steady state is reached when the heat absorbed in the primary circuit and transferred to the auxiliary circuit is the same; and the cold water circuit is used to obtain this equilibrium. And, all system depends on the refrigeration capacity from the auxiliary circuit to reach this balance.

Figure 6 shows the auxiliary circuit refrigeration capacity (W) in terms of evaporation temperature ($^{\circ}C$). Fig. 6 also shows the mass flow rate in function of the evaporation temperature. Looking at the mass flow and refrigeration capacity curves, it is possible to see that both are increasing when the evaporation temperature increases. It occurs because the refrigeration capacity depends strongly on the mass flow rate. Maia (1) explained this fact, justifying that the evaporation temperature increases at the same time as the pressure increases, and mass flow rate will be higher for a higher density, which causes an increase in the mass flow rate inside the compressor.

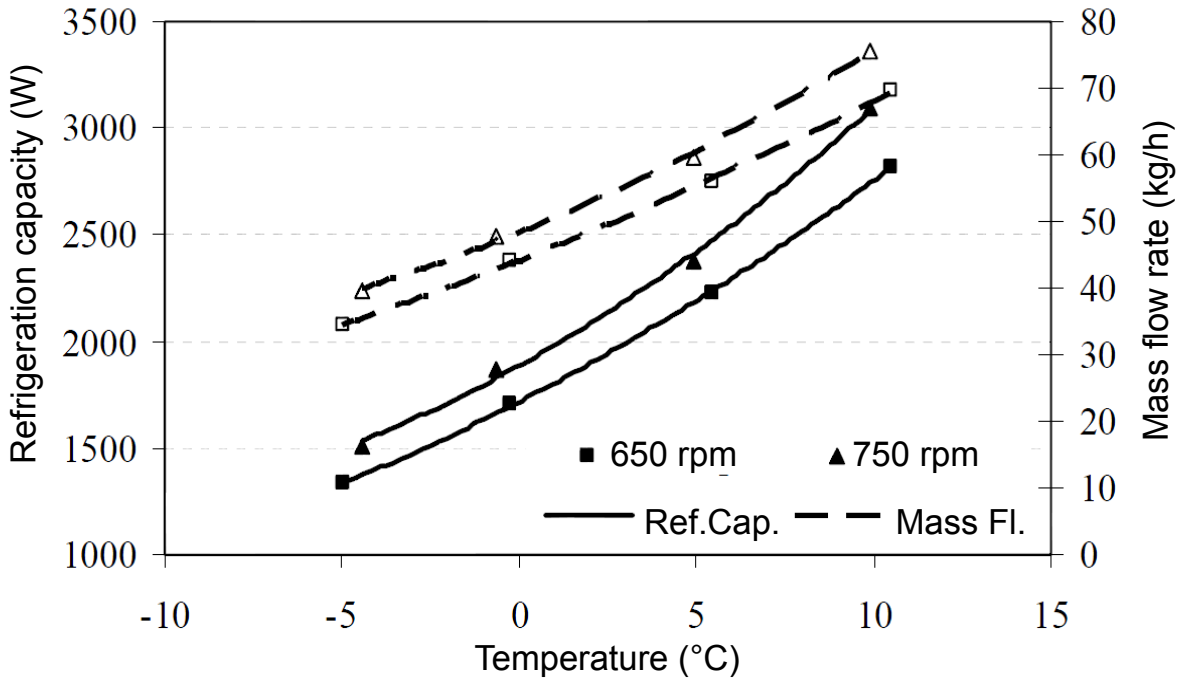

Figure 6 – Refrigeration capacity for the auxiliary circuit in function of evaporation temperature (1), using $50°C$ of condensing temperature.

Eq.1.10 presents the overall energy balance between the primary and auxiliary circuits:

$$\dot{Q}_{ace} = \dot{Q}_{ph} + \dot{Q}_{ts}, \tag{1.10}$$

where the heat transferred by the micro-pump and cold water pump were not considered; all tubes are considered adiabatic.

1.3 Experimental methodology

The choice of which steps follow during the experiments is made using the flow pattern map as a guide. During the change of pattern, the flow presents a change in saturated liquid distribution around the tube, and this will change the heat transfer as shown in greater details during the literature review section (see item 2). To obtain a data set with a large range of applicability, it is necessary to embrace all types of flow pattern.

The methodology presented by Wojtan et al. (23) was used to generate the Fig. 7, that shows a flow pattern map for the R-407C. The conditions used were $15°C$, 10 kW/m^2 and 20 liters per hour (lph). Volumetric flow meter was calibrate for water at standard

conditions, and volumetric flow in Fig. 7 was converted for this condition to facilitate the on-site correlation.

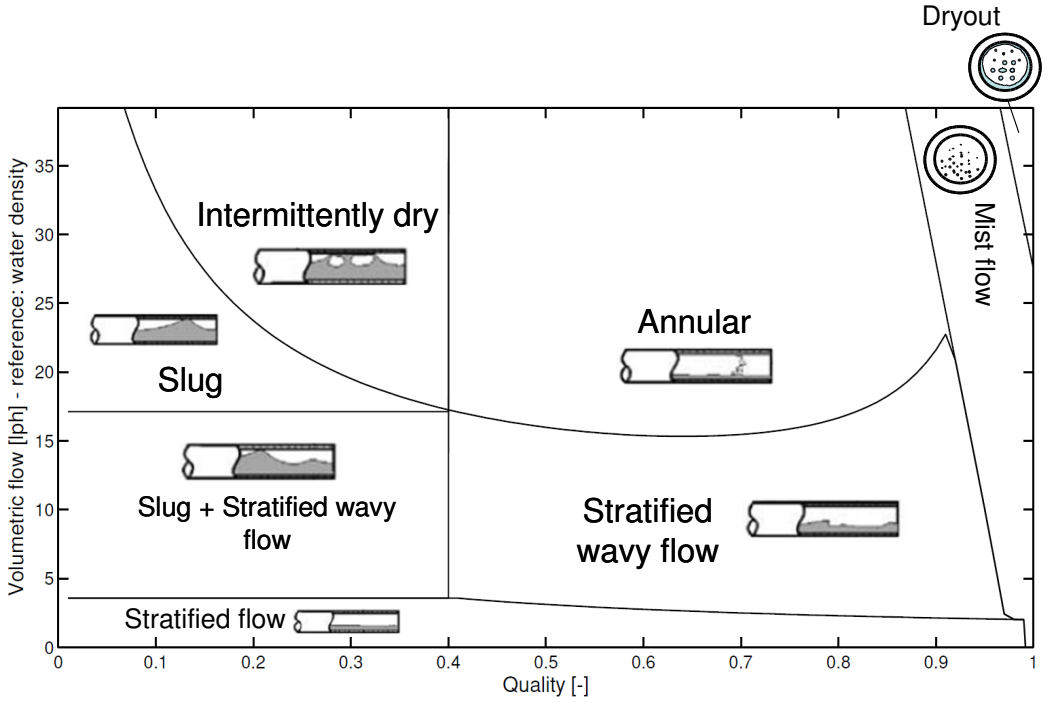

Figure 7 – Pattern flow map to the R-407C, at 15°C, 10 kW/m^2 and 20 lph: reference to the water.

For example, considering that the flow meter indicates 20 lph, it means that the fluid could be in the slug pattern, intermittently dry, stratified wavy flow, annular or mist flow, depending on the two-phase quality.

Using the experimental data sets presented in the Tab. 2, it is possible to obtain values for a large range of different conditions, including different types of flow pattern.

Table 2 – Experimental data sets for different operational conditions.

Experiment data set	Quality range	Heat flux ($kW\ m^{-2}$)	Volumetric flow (lph)
1	0.2 to 0.8	6	12, 18, 25
2	0.2 to 0.8	4	12, 18, 25
3	0.2 to 0.8	2	12, 18, 25

Electrical resistances x water in counter current

Favrat et al (24, 25) presented an experimental methodology using counter current instead of electrical resistances, to generate an uniform boundary condition on the test section. According Wojtan (26), for higher values of quality, there is a thermal conduction

along the copper tube on dryout transition region, that hides a peak value of heat transfer coefficient nearby, which does not occur when using counter current as the heating mechanism. In this work, electrical resistances are used, and it is not obtained values for the dryout region to avoid this problem.

1.3.1 Uncertainty analysis

Table 3 presents the calibration uncertainty, stability, resolution and distribution for the measuring instruments installed in the primary circuit and in the cold water circuit. These values will be used to generate the data set of heat transfer coefficient and for the inventory calculation, during the void fraction analysis.

Table 4 shows the uncertainty for the auxiliary circuit measuring instruments, and it was obtained from Maia (1). These values will be used during the balance of energy to the auxiliary circuit, and calculations that this circuit will be related with.

Table 3 – Uncertainty values for the primary and cold water circuit instruments.

Criteria	Thermocouple	Flow meter	Differential Pressure transmitter	Absolute pressure transmitter	Multimeter, $Current$ and $Voltage$
Calibration uncertainty	$\pm$ 0.30°C	-	$\pm$ 0.03kPa	$\pm$ 20.00kPa	$\pm$(2.50% + 35d), $\pm$ (0.80%+5d)
Stability	-	-	$\pm$ 0.02kPa	-	-
Resolution	-	$\pm$ 0.50 l/hr	-	-	-
Distribution	Rectangular	Uniform	Rectangular	Rectangular	Rectangular
Divisor	2	$\sqrt{3}$	2	2	

Table 4 – Uncertainty values for the auxiliary circuit instruments.

Criteria	Thermocouple	Flow meter	Absolute pressure transmitter for evaporator and condenser
Calibration uncertainty	$\pm$ 1.64°C	$\pm$ 1.35 kg/h	$\pm$ 60kPa and 370kPa

Folowing will be presented how the uncertainties are being calculated.

Methodology used for calculating the uncertainty

Following will be presented an example to demonstrate how the uncertainty is calculated for each one of pressure and temperature measurements.

Consider a thermocouple and an absolute pressure transmitter located in the test section. During steady state, it is recorded 45 measurements of temperature and pressure during one minute, as shown by Fig. 8. It is observed some expected variability, and this variability is taken into account during the expanded uncertainty calculation, as will be shown below.

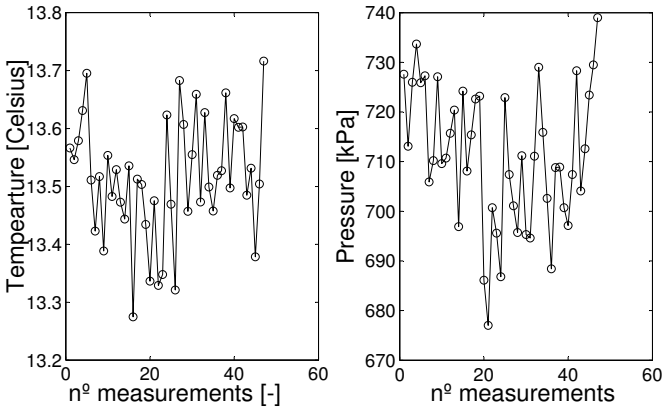

Figure 8 – Measurements of temperature and pressure, showing an example of the variability presented during the steady state experiments in the test section.

First step is obtaining an average for the 45 measurements presented in the Fig. 8, as shown by Eq. 1.11:

$$\begin{aligned} \bar{T} &= \frac{\sum_{i=1}^{N} T_i}{N} = 13.51\ ^{\circ}C, \\ \bar{P} &= \frac{\sum_{i=1}^{N} P_i}{N} = 711.17\ kPa, \end{aligned} \tag{1.11}$$

and, the standard deviation can be determined as:

$$\begin{aligned} s_T &= \sqrt{\frac{\sum_{i=1}^{N} (T_i - \bar{T})^2}{N}} = 0.1\ ^{\circ}C, \\ s_P &= \sqrt{\frac{\sum_{i=1}^{N} (P_i - \bar{P})^2}{N}} = 14.12\ kPa. \end{aligned} \tag{1.12}$$

Standard uncertainty is obtained dividing the standard deviation by the root square of the number of measurements, using the equation below:

$$\begin{aligned} u_1(T) &= 0.1\ ^\circ C/\sqrt{45} = 0.015^\circ C, \\ u_1(P) &= 14.12\ kPa/\sqrt{45} = 2.10kPa. \end{aligned} \tag{1.13}$$

The calibration uncertainty is presented by the manufacturer multiplied by the coverage factor of 2. To correct this expanded uncertainty to obtain the standard uncertainty:

$$\begin{aligned} u_2(T) &= 0.3\ ^\circ C/2 = 0.15^\circ C, \\ u_2(P) &= 20\ kPa/2 = 10.06kPa. \end{aligned} \tag{1.14}$$

The combined uncertainty is obtained using a summation in quadrature of the standard uncertainty presented in Eq. 1.14, plus the calibration uncertainty presented in the Table 3:

$$\begin{aligned} uc(T) &= \sqrt{u_1(T)^2 + u_2(T)^2} = \sqrt{0.015^\circ C^2 + 0.15^\circ C^2} = 0.15^\circ C, \\ uc(P) &= \sqrt{u_1(P)^2 + u_2(P)^2} = \sqrt{(2.1kPa)^2 + (10kPa)^2} = 10.22kPa. \end{aligned} \tag{1.15}$$

The degrees of freedom for these measurements are calculated as below:

$$\begin{aligned} v_{ef}(T) &= \frac{uc(T)^4}{\frac{u_1(T)^4}{v_T} + \frac{u_2(T)^4}{\infty}} = \frac{0.15^\circ C^4}{\frac{0.015^\circ C^4}{45-1} + \frac{0.15^\circ C^4}{\infty}} = 408738, \\ v_{ef}(P) &= \frac{uc(P)^4}{\frac{u_1(P)^4}{v_P} + \frac{u_2(P)^4}{\infty}} = \frac{10.06kPa^4}{\frac{2.10kPa^4}{45-1} + \frac{10.06kPa^4}{\infty}} = 24464, \end{aligned} \tag{1.16}$$

where v_T and v_P are the degree of freedom for the temperature and pressure, respectively. They are obtained from the number of measurements (45) minus one, for both temperature and pressure. Table 5 gives the coverage factor k_{95}, using the effective degrees of freedom (v_{ef}) obtained from Eq. 1.16. For higher values of degrees of freedom as shown in Eq. 1.16, the coverage factor will be approximately 2, representing a confidence level of 95%, and the expanded uncertainty will be determined as:

Table 5 – Student t-factor to determine the coverage factor for a level of confidence of 95%.

v_{ef}	1	2	3	4	5	6	7	8	10	20	50	100	∞
k_{95}	13.97	4.53	3.31	2.87	2.65	2.52	2.43	2.37	2.28	2.13	2.05	2.02	2

$$\begin{aligned} uc(T)_{95\%} &= uc(T)\ k_{95}(T) = (0.15^\circ C) \cdot (2) = 0.3^\circ C, \\ uc(P)_{95\%} &= uc(P)\ k_{95}(P) = (20.11kPa) \cdot (2) = 20.12kPa. \end{aligned} \tag{1.17}$$

And, the temperature and pressure can be finally expressed as:

$$\begin{aligned} T &= \bar{T} \pm uc(T)_{95\%} = 13.51\ ^{\circ}C \pm 0.3^{\circ}C, \\ P &= \bar{P} \pm uc(P)_{95\%} = 711.17\ kPa \pm 20.12kPa. \end{aligned} \tag{1.18}$$

It is possible to conclude that the results presented high precision, and the expanded uncertainty is basically the calibration uncertainty multiplied by the coverage factor.

For flow meter and multimeter, just one measurement was taken during the experiments; also, the resolution must be taken into the account. The standard uncertainty will be equal to the resolution over the cube root, plus the calibration uncertainty, using Eq. 1.14, Eq. 1.15, Eq. 1.17 and Eq. 1.18, as used here for temperature and pressure.

Software EES was used to calculate the uncertainty propagation, and the methodology implemented can be seen in the EES's manual (27).

1.4 Validating the test section quality and energy balance at the pre-heater

As R-407C is a zeotropic fluid, it is not necessary calculating the quality using an energy balance for the pre-heater and test section, as required for a pure fluid. The thermodynamic state inside the test section can be determined just using the temperature and pressure measurements in the test section. On the other hand, in order to validate thermodynamic state in the test section, values of quality using both methodologies can be correlated.

The quality can be calculated using a control volume on the pre-heater, by the following energy balance Eqs.1.19 and 1.20:

$$\dot{Q}_{ph} = \dot{m}_{R407c}\, \Delta i_{ph} = \dot{m}_{R407c}\, (i_7 - i_5) \therefore i_7 = i_5 + \frac{\dot{Q}_{ph}}{\dot{m}_{R407c}}, \tag{1.19}$$

and,

$$x_1 = \frac{i_7 - i_l}{i_v - i_l}, \tag{1.20}$$

where $\dot{m}_{R407c}$ is the R-407C mass flow rate, Δi_{ph} is the enthalpy difference between the pre-heater's inlet (T_5 and P_4, see Fig. 2) and outlet (P_6); i_l and i_v are the enthalpy in the saturated liquid and vapor, respectively. The enthalpies i_l and i_v, can be calculated using

the state equations for R-407C, as a function of quality and P_6:

$$\begin{aligned} i_l &= f(x = 0, P_6), \\ i_v &= f(x = 1, P_6). \end{aligned} \tag{1.21}$$

An alternative method to calculate the quality by Eq. 1.20 is using the state equations for the R-407C, in function of T_7 and P_6:

$$x_2 = f(T_7, P_6). \tag{1.22}$$

Comparing x_1 and x_2 is possible to validate the quality in the test section. Also, it is possible to determine which method has the lower uncertainty. For example, an experiment was made using the following properties:

- $T_5 = (10.96 \pm 0.31)°C$,
- $P_4 = (817.28 \pm 20.88)kPa$,
- $T_7 = (13.54 \pm 0.31)°C$,
- $P_6 = (816.65 \pm 20.95)kPa$,
- $\dot{m}_{R-407C} = (25 \pm 0.5)\, liters/hr$,

and, the results obtained were:

- $x_1 = 0.2274 \pm 0.01011$,
- $x_2 = 0.2176 \pm 0.1278$.

First, the results show that the energy balance in the pre-heater is well satisfied; second, these results demonstrate that the uncertainty is higher when using the temperature T_7 as a source, because a low variation in the temperature can cause a larger propagation during the uncertainty calculation, because of the glide. Following, it will be shown a section to present the main characteristics of the refrigerant fluid used in this work, the R-407C.

1.5 Refrigerant fluid R-407C

The R-407C is the zeotropic fluid used during this work. It is a zeotropic mixture comprised of three different fluids, R-32, R-125 and R-134a, in proportion of 23%, 25%

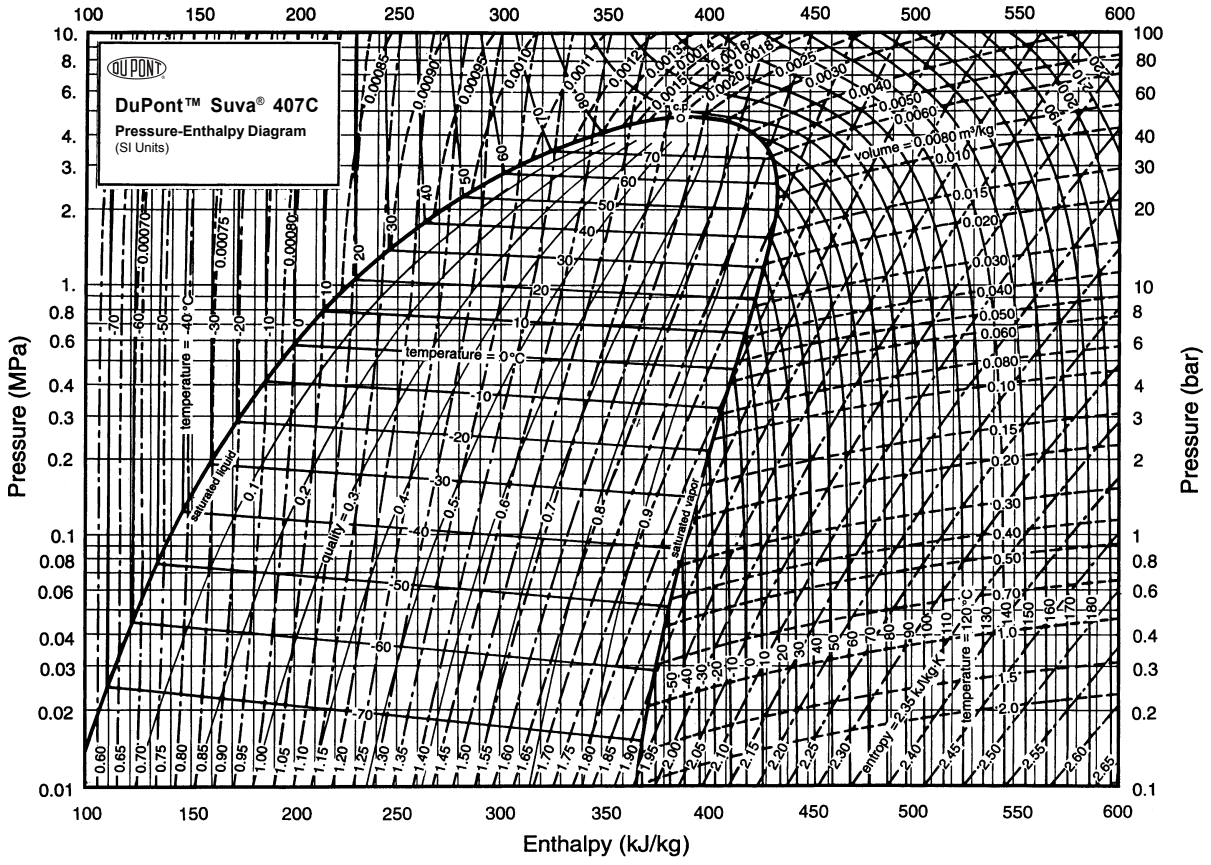

Figure 9 – Pressure versus Enthalpy diagram for the R-407C.

and 52%, respectively, containing no ozone-depleting chlorine. Figure 9 shows a pressure-enthalpy diagram for the R-407C, provided by the manufacturer DuPont.

A zeotropic mixture is that one in which temperature change is observed at constant pressure during phase change. Latini (28) classifies a fluid as zeotropic if this temperature variation is greater than $5°C$. Zeotropic fluids also have the quality of being distillable, and also the proportion between the fluids can change inside the refrigeration system depending on the thermodynamic state. Another important issue occurs during recharge, because it is difficult predicting the exactly amount of fluid inside the system, and the composition of this one. R-407C is indicated as one of the most important candidate to replace the R-22, because they have similar properties at operational points.

Looking at Table 6, it is possible to see the relation between pressure, saturation temperature and glide for the R-407C. In this work, the test section pressure will range between 700kPa to 1100kPa, which means that the temperature will vary between $6.7°C$ to $28.96°C$, and the glide will be approximately constant, equals to $6°C$. In consequence of this glide, the evaporation temperature will increase along the test section, and this relation is considered linear, $\Delta T = 6°C\ \Delta x$; for example, considering $\Delta x = 1\%$, ΔT will be $0.06°C$. Considering that the absolute uncertainty is equal to approximately $0.3°C$, it

will be difficult to realize quality changes for less than 5%, accurately.

Table 6 – Glide to be observed for the pressure range used during the experiments.

Pressure, kPa	Temperature, $°C$ (x=0)	Temperature, $°C$ (x=1)	Glide, $°C$
700	6.708	13.08	6.376
800	11.13	17.42	6.283
900	15.16	21.34	6.183
1000	18.86	24.94	6.076
1100	22.3	28.26	5.963

1.6 Conclusion

In this chapter was presented the experimental device used in this work, highlighting the balance of energy in each circuit and the overall energy balance between the primary and auxiliary circuit. The experimental methodology was also presented, showing how the experiments were organized. The uncertainty analysis and a validation in the thermodynamic state at the test section were shown, based on a control volume on the pre-heater, and applying the energy balance between the pre-heater's inlet and outlet. And, in the last one section, the zeotropic fluid used, R-407C was presented, showing the most important characteristics, and presenting relevant works that used this refrigerant mixture.

Part II

Methodology and literature review

2 Methodology and literature review

2.1 Literature review on coefficient of heat transfer relations

Understanding the different phase change flow regimes is critical to the development of HTC correlations. Phase changing has multiple roles in HVAC, and what is particularly relevant in our study is the enhancing mechanism for heat transfer capacity. In general, heat transfer rates during phase change can be 4 to 25 times higher than for equivalent single-phase forced convection (29). Figure 10 describes the most relevant flow patterns and HTC levels during the phase change process along an evaporator tube. The flow pattern presented in this figure is only illustrative and it will vary depending on the fluid characteristics and flow regimes (evaporation temperature, vapor pressure, heat flux, mass flow velocity, diameter and vapor quality, *etc.*) Observing the evolution of HTC regimes along the evaporator it is possible to recognize:

- a gradual increase in HTC due to the phase change phenomena, related to nucleate and convection boiling;
- a rapid decrease for high values of quality, more precisely in the region identified as dryout/mist flow.

The phase change mechanism can be further divided into two different processes: convection boiling, which is the phase change regime that occurs in the liquid/vapor inter-

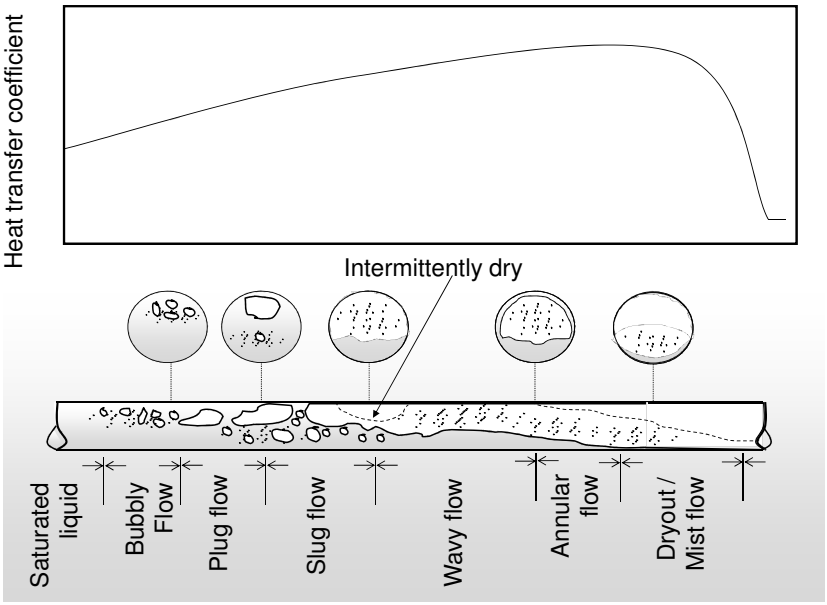

Figure 10 – Example of a phase change inside a fluid passing through a tube evaporator.

face, and nucleate boiling, which is the phase change regime related to bubble formation on a heated surface (liquid/solid interface). There is a group of correlations, called Strictly Convective, that considers only the convection term during the calculation of a two-phase flow HTC (30, 31, 32, 33, 34, 35, 36). In general, Strictly Convective correlations use the well-known Dittus-Boelter heat transfer relation applied to saturated liquid flow and the Martinelli parameter (37), as expressed by:

$$h_{tp} = h_l(1 + C_l\chi_{tt})^{-C_2}, \tag{2.1}$$

where C_1 and C_2 are constants obtained empirically, as proposed by Bandarra (36). Another group of correlations, called Superposition Rule correlations, considers both processes: convection boiling (h_{cb}) and nucleation boiling(h_{nb}) (38, 4, 39, 6, 40, 41). These correlations determine the functional form of the HTC by weighing the contribution of each mechanism of heat transfer (h_{nb} and h_{cb}) as:

$$h_{tp} = [(Fh_{cb})^n + (Sh_{nb})^n]^{1/n}. \tag{2.2}$$

In Eq. 2.2 the factors S and F are weighing factors for the two components. At high values of mass flow, the temperature gradient near the wall increases as consequence of a thinner boundary layer. The effective temperature around bubbles also decreases reducing the chances of new bubble formation. In this situation the suppression factor S becomes smaller. Likewise at high vapor quality flow regimes there is a smaller chance of bubble formation, and the suppression factor S should again decrease. Otherwise, the convective heat transfer should increase for high values of quality and mass flow, and the factor F, composed by the Martinelli parameter χ should express it. When the parameter n is not equal to unity, the weighing is biased, and the result tends to become closer to the largest value among the two terms. Generally speaking, Superposition Rule correlations produce more robust and useful approximations than Strictly Convective correlations.

A third group of two-phase flow approximations for HTCs is the so-called Strictly Empirical (42, 5, 43). In this group dimensionless numbers are correlated to experimental data using numerical methods for optimization of the coefficients. This technique has gained popularity (44, 45) with the increase of computational power in recent years that enables testing large quantity of dimensionless numbers and increasingly complex data sets.

The fourth group of HTCs is closely related to the flow pattern map. As shown in Fig. 10 there are substantial differences between the different flow regimes along the tube, and for this reason several authors have investigated flow pattern maps to propose HTC correlations for each flow pattern (30, 46, 47, 24, 25, 23, 26), instead of a single global correlation. Fig. 11 shows an example of flow pattern map implemented using the methodology presented by Wojtan et al. (23). The subjective aspect of pattern

determination (48) has been greatly mitigated by new methodologies, as presented by Ursenbacher et al. (49). The main drawback of using Wojtan et al. (23, 26) methodology is the assumption of *a priori* knowledge of the heat flux, which is typically what the designer is trying to determine in the first place.

In this work is tested different correlations to verify which one will predict better the HTC for the R-407C.

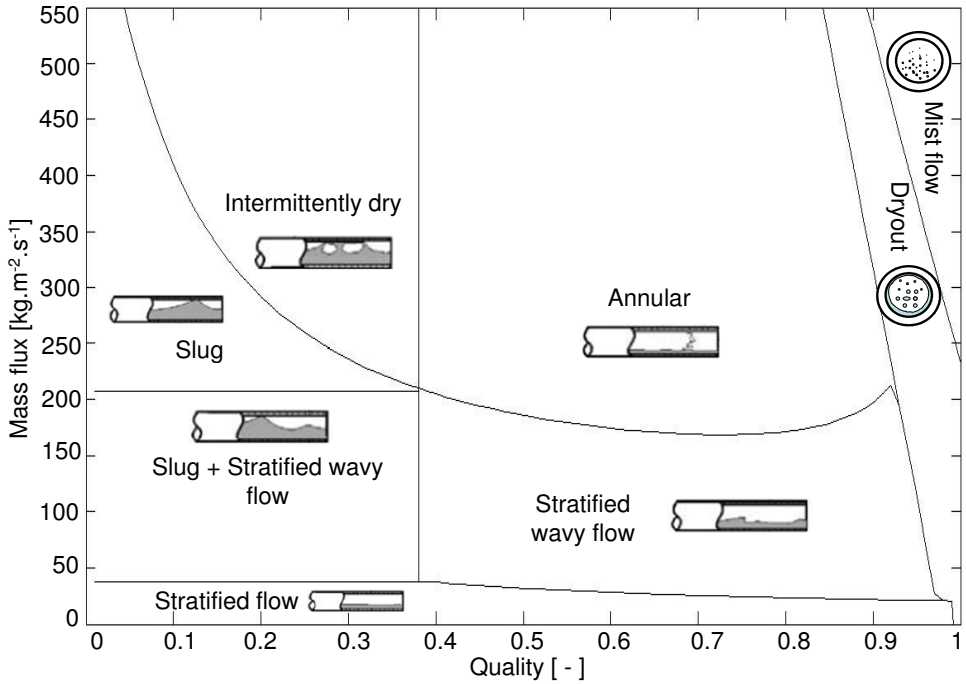

Figure 11 – Flow pattern map for refrigerant R-22 for saturation temperature of 8°C, an internal diameter of 12.97 mm, and heat flux of 5 kWm^{-2}.

2.1.1 Heat transfer coefficient relations used in this work

The relations of Kandlikar (5), Gungor and Winterton (4) and Watellet (6) were used to test the correlation with the experimental data, and these relations can be found in Tab. 7.

Kandlikar (5) relation was used here because it is a well-known relation, and also represents the strictly empirical relations group. Gungor and Winterton (4) relation is used because it has a good agreement with the experimental data, and this makes part of the group of superposition effect relations. Watellet (6) was used because it has a great acceptance in the scientific community, and also makes part of the superposition effect relations.

Table 7 – Heat transfer coefficient relations used in this work.

Author	Correlation
Kandlikar (5)	$h_{tp} = h_l \left[C_1 Co^{C_2} (25 Fr_l)^{C_5} + C_3 Bo^{C_4} F_{fl} \right]$
	Convective region: $C = \left[1.136, -0.9, 667.2, 0.7, 0.3 \right]$
	Nucleate boiling region: $C = \left[0.6683, -0.2, 1058.0, 0.7, 0.3 \right]$
	$F_{fl} = 2.2$, considered the same as R-22
Gungor and Winterton (4)	$h_{tp} = h_l \left[1 + 3000\, Bo^{0.86} + 1.12 (\frac{x}{1-x})^{0.75} (\frac{\rho_l}{\rho_v})^{0.41} \right]$
Watellet (6)	$h_{tp} = (h_{ec}^{2.5} + h_{nb}^{2.5})^{-2.5}$, where,
	$F_w = 1 + 1.925 \chi_{tt}^{-0.83}$
	if $Fr_l \leq 0.25$, $R_w = 1.32 Fr_l^{0.2}$
	if $Fr_l > 0.25$, $R_w = 1$
	$h_{ec} = F_w\, R_w\, h_l$
Parameters used in common:	$h_l = 0.023 Re_l^{0.8} Pr_l^{0.4} \frac{k_l}{d}$
	$Re_l = G\, \frac{d}{\mu_l} (1 - x)$
	$h_{nb} = 55 (P_r)^{0.12} (-log_{10}(P_r))^{-0.55} M^{-0.5} (\phi)^{0.67}$

2.2 Methodology to obtain general heat transfer coefficient relations for pure and azeotropic fluids

This section describes the methodology used to generate the new correlations. The first step in this process is to create a set of inputs that may or may not be included in the correlations. The first group of inputs takes the form of dimensionless numbers based on several properties d, U, k, μ and i_{lv}, and are determined through the Buckinham's Π theorem (50). Other inputs consist of the enhancing factor S presented in Lima (17) (see correlation number 4, Tab. A.1), and the dimensionless numbers given by Wojtan et al. (23, 26). The parameters C_1, C_2 to C_5 are also used here in order to consider the influence of the fluids' critical thermophysical properties in the HTC correlation. Tab. A.1 lists all the dimensionless numbers used to generate the relations. The second step is to determine the functional form for the correlation. Given that it is impossible to know beforehand what type of correlation performs best it is explored four functional forms for the HTC correlations: two strictly empirical algebraic equations, an algebraic equation based on the Superposition Rule and a correlation based on ANNs. The two empirical algebraic

correlations are given by:

$$h_{tp} = \left(\sum_{i=1}^{n_1} a_i X_i^{b_i} \right) \left(\prod_{j=1}^{n_2} X_j^{c_j} \right), \tag{2.3}$$

and,

$$h_{tp} = a_0 \sum_{i=1}^{n_1} a_i X_i^{b_i} + c_0 \prod_{j=1}^{n_2} X_j^{c_j}, \tag{2.4}$$

where the X's are a subset of the dimensionless parameters in Tab. A.1, and the coefficients a_i, b_i and c_j can be negative which means that these expressions can also include subtractions and divisions.

The third functional form is based on the Superposition Rule:

$$\begin{aligned} h_{tp} = & \Bigg[\left(a_0 \sum_{i=1}^{n_1} a_i X_i^{b_i} + c_0 \prod_{j=1}^{n_2} X_j^{c_j} \right) h_l^n] \\ & + \left(a_0 \sum_{i=1}^{n_1} a_i X_i^{b_i} + c_0 \prod_{j=1}^{n_2} X_j^{c_j} \right) h_{nb}^n \Bigg]^{1/n}, \end{aligned} \tag{2.5}$$

where h_l is the correlation of Dittus-Boelter applied for saturated liquid flow and h_{nb} is the nucleate boiling HTC correlation presented by Cooper (51).

For a given set of X the correlation's coefficients a_i, b_i and c_j are determined using an unconstrained line-search method (52) implemented in Matlab R2012b and accessible through the Optimization toolbox via the function $fminunc$. The optimization method searches for the coefficients that minimize the root mean squared error (RMSE) between the experimental HTC and Eq. 2.3, 2.4 and 2.5.

The fourth type of correlation considered is obtained through ANNs. ANNs are useful tools for approximating complicated mapping functions for problems in classification and regression (53) and have been used extensively in many areas. The advantage of ANNs is that no assumptions are required about the underlying process relating input and output variables. However, because ANNs are universal approximating functions, their mapping capabilities can potentially lead to problems such as over-fitting training data (53), and thus leading to poor generalization on new data sets. In this study the ANN is a representation of HTC in terms of a subset of the dimensionless parameters X. The ANN representation is based on signals being sent through elements called neurons in such a way that the processing of the inputs signals produces an output HTC or target value which in this case, are the experimental values for HTC. Neurons are arranged in layers, where the first layer contains the set of inputs, the last layer contains the output, and the layers in between (referred to as hidden layers) contain hidden neurons. The feedforward neural network that is used here, with N_i inputs and N_h neurons in one hidden layer and linear output activation function, can be expressed as

$$h_{tp} = a_0 \left[\sum_{i=1}^{N_h} w_i f^h \left(\sum_{j=1}^{N_i} w_{ij} \widetilde{X}_j + w_{i0} \right) + w_0 \right], \tag{2.6}$$

where f_i^h is a transfer function and $\widetilde{X_j}$ is the jth dimensionless parameter normalized in the range $[-1, 1]$ using the range limits listed in Table A.1. Numerical optimization algorithms such as back-propagation, conjugate gradients, quasi-Newton, and Levenberg-Marquardt have been developed to efficiently adjust the weights, w_i and w_{ij} and bias w_{i0} and w_0 in the feedforward neural network seeking to minimize a performance function like the mean squared error.

Table A.1 – Input parameters considered in the search for HTC correlations

X_i	Relation	Source	Range	X_i	Relation	Source	Range
1	$Re_{l,1} = G(1-x)\frac{d}{\mu_l}$		$[83, 33870]$	15	$P_8 = di_{lv}^{0.5}\frac{\rho_v}{\mu_{eq}}$		$[3\times10^{-3}, 5\times10^{-2}]$
2	$\chi_{tt} = (\frac{1-x}{x})^{0.875}$ $(\frac{\rho_v}{\rho_l})^{0.5}(\frac{\mu_l}{\mu_v})^{0.125}$		$[1.8, 118.6]$	16	$P_9 = \frac{dg}{i_{lv}^{0.5}}$	[30]	$[4.9\times10^5, 10^7]$
3	$Fr_l = \frac{G^2}{\rho_l^2 g \quad d}$	[29]	$[0.01, 1.6]$	17	$P_{10} = \frac{U_v}{U_l}$		$[6.4\times10^{-7}, 8\times10^{-7}]$
4	$UC_1 =$ $1 + 1.893\chi_{tt}^{-0.77}$		$[4.7\times10^{-3}, 3.0]$	18	$C_1 = \frac{P}{P_{crit}}$		$[0.09, 0.2]$
5	$Re_{l,2} = \rho_l U_l \frac{d}{\mu_{eq}}$		$[4.5\times10^3, 2.5\times10^5]$	19	$C_2 = \frac{\rho_v}{\rho_{crit}}$		$[0.03, 0.1]$
6	$Pr_{eq} = \mu_{eq}\frac{cp_{eq}}{k_{eq}}$		$[2.5\times10^{-4}, 11.1]$	20	$C_3 = \frac{\rho_{eq}}{\rho_{crit}}$	Present	$[0.18, 2.7]$
7	$P_1 = \frac{i_{lv}}{U_l^2}$		$[7.7\times10^5, 1.4\times10^8]$	21	$C_4 = \frac{\rho_v}{\rho_{crit}}$	work	$[2.1, 2.75]$
8	$P_2 = \frac{\sigma}{U_l \mu_{eq}}$		$[119.5, 7084]$	22	$C_5 = \frac{T_l}{T_{crit}}$		$[0.06, 0.16]$
9	$Re_{l,3} = \rho_l U_v \frac{d}{\mu_{eq}}$		$[27.8, 70.2]$	23	$\epsilon =$ $\frac{x}{\rho_v}\{[1+0.12(1-x)](\frac{x}{\rho_v}+$ $\frac{1-x}{\rho_l})+$ $\frac{1.18(1-x)[g\sigma(\rho_l-\rho_v)]^{0.25}}{G\rho_l^{0.5}}\}^{-1}$		$[0.46, 1]$
10	$P_3 = \frac{dg}{U_l^2}$	[30]	$[1.8\times10^5, 1.2\times10^7]$	24	$x_{IA} = \{[0.291(\frac{\rho_v}{\rho_l})^{-0.571}$ $(\frac{\mu_v}{\mu_l})^{-0.143}]+1\}^{-1}$	[26]	$[0.32, 0.43]$
11	$P_4 = \frac{di_{lv}^{0.5}\rho_l}{\mu_{eq}}$		$[0.62, 9.0]$	25	$Q_{crit} =$ $\frac{0.131\rho_v^{0.5} i_{lv}[g\sigma(\rho_l-\rho_v)]^{0.25}}{W m^{-2}}$		$[3.6\times10^5, 4.75\times10^5]$
12	$P_5 = \frac{U_l}{i_{lv}^{0.5}}$		$[3.3\times10^7, 3.3\times10^8]$	26	$Bo = \frac{\phi}{G i_{lv}}$	[29]	$[5\times10^{-5}, 1.3\times10^{-5}]$
13	$P_6 = \frac{\sigma}{i_{lv}^{0.5}\mu_{eq}}$		$[8.6\times10^{-5}, 1.1\times10^{-3}]$	27	$h_l = 0.023 Re_l^{0.8} Pr_l^{0.4}\frac{k_l}{d}$		$[7, 943]$
14	$P_7 = \frac{U_v}{i_{lv}^{0.5}}$		$[0.1, 1]$	28	$h_{nb} =$ $55P_r^{0.12}(-logP_r)^{-0.55}\times$ $M^{-0.5}q^{0.67}$	[31]	$[1180, 4377]$

The correlations given by these expressions are uniquely determined by the inputs X used and the several free coefficients (a_i, b_i, c_i, w_{ij}, *etc.*). In the case of Eq. 2.3, 2.4 and 2.5 each input can appear multiple times in the correlation, once for each term. The correlations' inputs are controlled by the binary vector $\vec{x}$ whose elements control the inclusion ($\vec{x}_i = 1$) or exclusion ($\vec{x}_i = 0$) of the dimensionless parameters X. For the ANN-based correlation is also needed to stipulate the number of neurons and the type of transfer function used. That is done by appending 2 integer elements binary vector $\vec{x}$. The first in the range $[5, 20]$ determines the number of neurons N_h in the hidden layer and

the second in the range $[1, 4]$ is used to select the transfer function f^h out of 4 possibilities: hyperbolic tangent sigmoid transfer function, log-sigmoid transfer function, radial basis transfer function or the linear transfer function.

The best correlation for each one of the for types here explored is be the one one that minimizes the RMSE:

$$\underset{\vec{x}}{\operatorname{argmin}} \sqrt{\frac{1}{N}\sum_{i=1}^{N}\left(h_{tp,exp,i} - h_{tp,i}(\vec{x})\right)^2}, \tag{2.7}$$

where $h_{tp,exp}$ is the experimental HTC, and h_{tp} is the HTC computed by the new correlations defined by the vector $\vec{x}$.

The minimization problem given by Eq. 2.7 is achieved with a genetic algorithm (GA). Gradient-based optimization methods are not suited for this problem because it is not trivial to compute the gradient of Eq. 2.7 with respect to $\vec{x}$. The GA is a space search technique based on the mechanism evolution and survival of the fittest (54). In this algorithm the evolution starts with a population of individuals (determined by vectors $\vec{x}$). Each individual in the population is ranked according to the RMSE Eq. 2.7, between the experimental and the calculated HTC values. The initial population is evolved based on the selection, crossover and mutation operators with the objective to minimize RMSE. Crossover operates on individuals (parents) determined by the selection operator that selects individuals for crossover based on fitness. In this method is used the stochastic uniform methods to select individuals for crossover, in this method the probability of selection is proportional to the individuals' fitness. Crossover recombines the genetic material of the selected parents. This method uses the scattered method in which a random binary vector with the same length as $\vec{X}$ is used to select the elements coming from each parent. The crossover operator selects elements from the first parent where the vector has 0 entries and selects genes from the second parent when it has 1 entry. The mutation operator modifies individuals that have not been selected for reproduction by randomly changing $\vec{x}$. In this method is used the uniform mutation algorithms that selects a fraction of the vector $\vec{x}$ for mutation and each of these entries has a 5% probability mutated. If the entry is mutated, each selected entry is replaced by a uniformly random entry. Once the population for a new generation is determined this process continues until some criterion is met. Given that it is difficult to formally specify a convergence criterion for the genetic algorithm due to its stochastic nature, and the algorithm stops after 100 generations or if no improvement has been observed over a pre-specified number of generations, in this case 50, whichever happens first.

2.2.1 HTC zeotropic degradation

Zeotropic mixtures present a heat transfer degradation as a result of mass transfer resistance and this phenomenon is discussed in greater details by Venter (55). During

phase change, the more volatile fluid becomes vapor first and at a higher velocity rate than the less volatile, and as consequence of this fact the saturate liquid becomes richer in a higher boiling point fluid; this change on the liquid fraction composition of the mixture causes an increase on the wall superheating for the same heat flux, causing a decreasing on the HTC. According Venter (55) the degradation becomes more pronounced for higher pressure and heat flux, and for a determined concentration in the equilibrium of phases. Several authors have been studying the degradation on nucleate boiling HTC in mixtures (55, 2, 56, 57, 58, 59, 60, 61, 62, 63, 64, 65, 66, 67, 68, 69).

Schlindwein et al. (69) more recently have used a methodology in which a reduction factor is applied on the HTC pure fluid relation to obtain the HTC relation for mixtures. The reduction factor applied on the nucleate boiling has the following functional form:

$$\frac{h_{nb,m}}{h_{nb,p}} = \frac{1}{1+K}, \tag{2.8}$$

where, $h_{nb,m}$ is the mixture nucleate boiling HTC, $h_{nb,p}$ is the pure fluid nucleate boiling HTC, and K is the reduction factor. The same methodology will be applied in this work.

Lee et al. (2) indicate that the temperature profile in a mixture is different from a pure refrigerant, and this difference was presented as depicted in Fig. 12. Lee et al. proposed using this approach to take into account the degradation effects. A reduction factor was proposed:

$$h_m = \frac{h_p}{1+K} = \frac{h_p}{1+\frac{h_{pure}(T_{int}-T_l)}{\dot{Q}"}}, \tag{2.9}$$

and,

$$T_{int} = T_v - (1-x)(T_v - T_l), \tag{2.10}$$

where T_{int} is the temperature at liquid/vapor interface; h_p is the HTC calculated by relations developed for a pure fluid and h_m is the HTC corrected for mixtures.

Looking at Eq. 2.9 and Eq. 2.10 is possible to see that the correlation proposed by Lee et al. (2) applies the reduction factor to the overall HTC (convective and nucleate boiling), and does not do it just for nucleate boiling as indicated by Schlindwein et al. (69). Also, this relation was proposed for condensation, and this present work is applied for evaporation phenomenon.

Gorenflo (56) presented a review on pool boiling, showing aspects related to the degradation caused by mixtures on nucleate boiling HTC. A reduction factor is applied as below:

$$K = \left(T_{int} - T_s\right)/\Delta T_{id}, \tag{2.11}$$

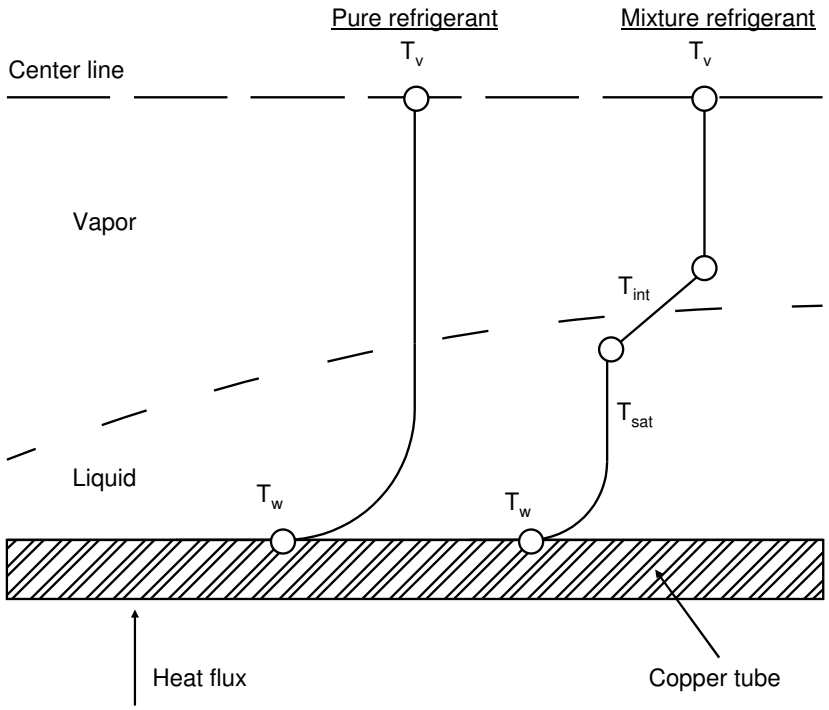

Figure 12 – Comparison between the temperature profile in a pure refrigerant and in a mixture according (2).

and,

$$\Delta T_{id} = \dot{Q}"/h_{nb,p}, \tag{2.12}$$

and,

$$\Delta T_{id} = \sum x_j \Delta T_j, \tag{2.13}$$

and,

$$T_{int} - T_s \approx \sum T_{sj}(x_j - y_j)(1 - exp(-B\dot{Q}"/\rho\beta\Delta h_{lv})), \tag{2.14}$$

where x and y are the molar fraction of liquid or vapour, β is the mass transfer coefficient, ρ and Δh_{lv} are density and heat of vaporization, and B is a fitting parameter, and β is the mass transfer coefficient.

Thome (57) proposed the following approximation:

$$K = \frac{h_{nb,p}}{\dot{Q}"}\Delta T_{bp}\left(1 - exp\frac{-\dot{Q}"}{\rho_l\, h_{lv}\beta}\right), \tag{2.15}$$

where β is fixed at 0.0003 m/s and ΔT_{bp} is the total glide. The relation presented by Thome will be used in the next chapter to evaluate the reduction on the nucleate boiling HTC for the R-407C.

2.3 Inventory and void fraction

2.3.1 Introduction

The inventory of a refrigeration system is the amount of refrigerant mass distributed between the components (evaporator, condenser, compressor, expansion device, tubing, *etc.*) in the refrigeration equipment, and it reflects the refrigerant charge that is in place before the system starts working.

The manufacturers generally provide the mass that should be charged in the equipment, because the equipment operates more reliably with this specific charge. Occasionally, the system needs to be recharged, and this practice should be performed in a manner that guarantees that the same amount of refrigerant is inside the equipment as there was at the first charge.

However, it is a common practice to charge equipment sub-optimally, which can result in many adverse consequences:

1. The equipment has a different COP when charged with more or less fluid (70, 71, 72);
2. Higher charge results in fluid being wasted, and in higher emissions of HCFCs and HFCs in the planet's atmosphere, which has greenhouse effect consequences;
3. Incorrect refrigerant charge is also related to compressor failures;
4. A charge higher than optimal can result in liquid entering the compressor and causing failure (optimal charge results in a superheated state at the end of the evaporator tubing). On the other hand, a low charge is associated with excessive superheating, which decreases the compressor's lifetime (by increasing the compressor discharge temperature).

The best method to determine the correct refrigerant charge is to calculate it. Basically, refrigeration system inventory depends on the equipment size (internal volume), the thermodynamic state of the fluid inside the components (evaporator, condenser, tubing and others), and the environmental conditions. In this work, the analysis is focused on the evaporator and the condenser because these are the components where phase change occurs.

Simplified methods to calculate the inventory have been discussed by Dmitriev and Pisarenko (73) for domestic refrigerator units charged with R-12. They suggested a relation that primarily depends on the volumes of the evaporator and condenser.

Otaki (74) developed a classical method to determine the mass inside a refrigerant system in which the mass distribution is obtained from the energy balance between the

secondary fluid (air, water or another fluid) and the single-phase fluid in the evaporator (vapor) and condenser (vapor and liquid). Correlations for determining the heat transfer coefficients are critical to this approach, and can be obtained from the literature (29, 75, 76). Otaki tested the method for several refrigeration systems, and the average error between the prediction and the actual inventory was 10%. In fact, the success of the Otaki method depends on the existence of correlations for the external heat transfer coefficient in the literature. These correlations are difficult to find for some new heat exchangers, such as the evaporator shown in Fig. 13; therefore, inventory estimation using Otaki's method is difficult for such equipment.

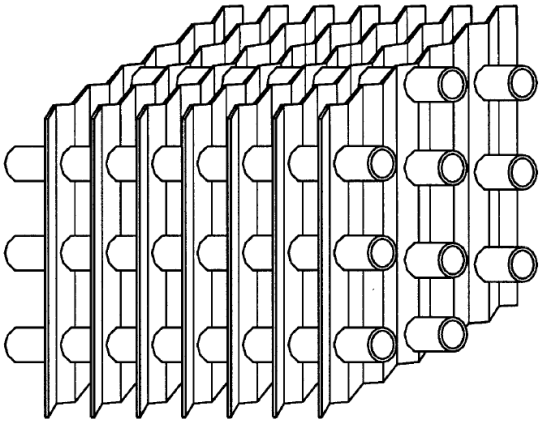

Figure 13 – Example of an air evaporator with detailed and uncommon external geometry (3).

In this work is also presented an alternative method for predicting the refrigeration system inventory, whereby the refrigerant mass in a heat exchanger (condenser and evaporator) can be predicted without specific knowledge of external heat transfer coefficient. In contrast, the evaporation (boiling) and condensation heat transfer coefficients are required in the proposed method. Because this new methodology is based on the Otaki method, it will be referred to as the 'modified Otaki' method.

The modified Otaki method was recently validated in (77) for pure fluids, and will be also used here to be validated for mixtures.

2.3.2 Otaki method

To introduce the Otaki method, consider refrigerant flow in counter current with water (as a secondary fluid) in an evaporator, as shown in Fig. 14. A control volume involving the refrigerant tubing (at the superheated region), allows us to determine the energy balance between the refrigerant side and the water side. Thus, the application of the first law of thermodynamics to this control volume results in Eqs.2.16 and 2.19.

$$Q_{sh} = \dot{m}_r \, (i_{r2} - i_{r3}) = \dot{m}_s \, cp_s \, (T_{s1} - T_{s3}), \tag{2.16}$$

and,

$$Q_{sh} = U_{sh}\, S_{sh}\, \Delta T_{sh}, \tag{2.17}$$

and,

$$U_{sh} = \left(\frac{1}{h_r} + R_w + \frac{1}{h_s\, R_S} \right), \tag{2.18}$$

and,

$$\Delta T_{sh} = \frac{[(T_{s3} - T_{r1}) - (T_{s1} - T_{r2})]}{ln\left[\frac{T_{s3} - T_{r1}}{T_{s1} - T_{r2}}\right]}, \tag{2.19}$$

where Q_{sh} is the heat transfer rate from the secondary fluid to the refrigerant, $\dot{m}_r$ is the refrigerant mass flow, and $\dot{m}_s$ and cp_s are the mass flow and the specific heat of the secondary fluid, respectively. Additionally, i_{r3} and i_{r2} are the refrigerant enthalpies, T_{s1} and T_{s3} are the secondary fluid temperatures at the entrance and exit, respectively, and S_{sh} and ΔT_{sh} are the heat transfer surface area and logarithmic mean temperature difference, respectively. U_{sh} is the global heat transfer coefficient, which is a function of h_r and h_s (heat transfer coefficients of the refrigerant and secondary fluid, respectively), R_w is the wall thermal resistance (between the refrigerant and secondary fluid) and R_s is the surface ratio (between the secondary surface area and the refrigerant surface area). All of the above quantities refer exclusively to the superheating region, except for $\dot{m}_r$ and $\dot{m}_s$, which are constant throughout the heat exchanger, and cp_s, which varies slightly.

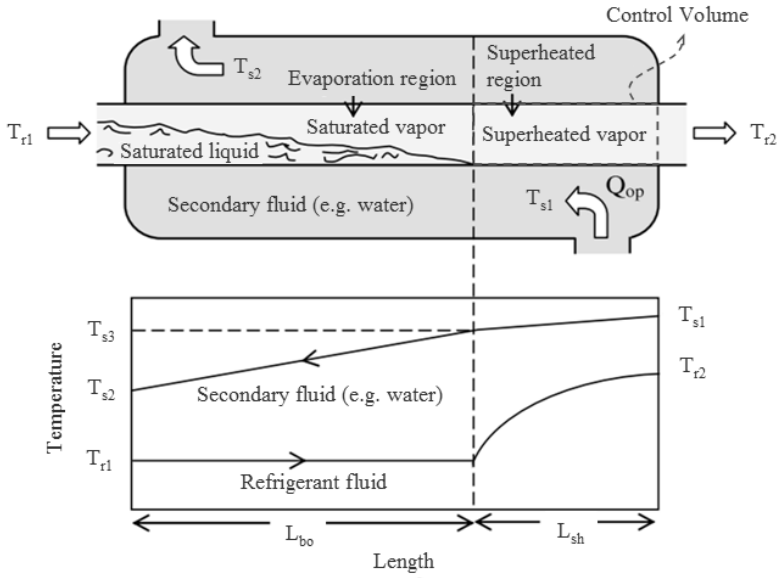

Figure 14 – Counter-flow evaporator and temperature-length graph of the refrigerant and secondary fluid.

The first step to use the Otaki Method is to calculate the heat transfer coefficient of the secondary fluid and the one-phase fluid (superheated). Values of the coefficients h_r and h_s can be estimated from literature using the classical Dittus-Boelter correlation, which is valuable for turbulent flows (29). Afterwards, the Eq. 2.18 should be used to determine U_{sh}.

The second step is to perform the energy balance in the one-phase region. With the values of Q_{sh}, U_{sh} and ΔT_{sh} (obtained by Eqs. 2.16, 2.18 and 2.19, respectively), the heat transfer surface area Ssh can be obtained by Eq. 2.17, and the superheating region length can be easily found.

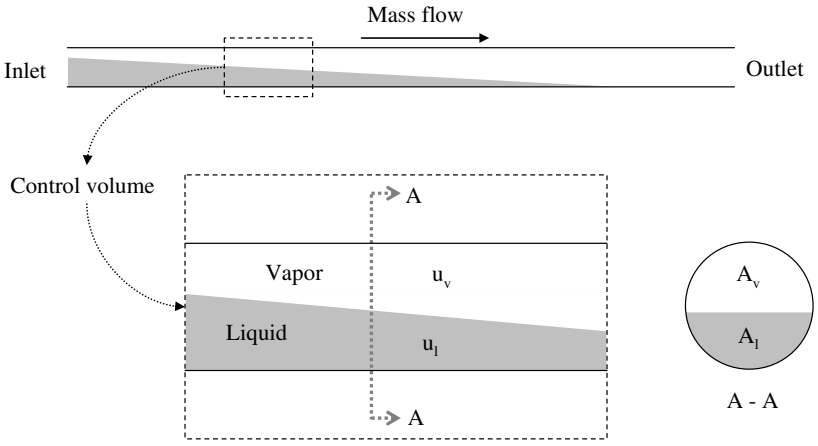

Figure 15 – Control volume and vapor and liquid distributions in a cross-section in a two-phase flow (e.g. evaporation region).

The third step is to calculate one and two-phase flow region lengths. The Otaki method uses the energy balance to obtain the length of the one-phase (superheating) region of the evaporator (it is possible because all the other terms are known). The evaporator total length is also known (if it is a well defined design), so the two-phase (evaporation) region length can be obtained by subtracting the one-phase length from the total length (therefore the one and two-phase volume is also known).

To finish the mass calculation is necessary use the calculated volumes and determine the mass. The vapor mass in the superheating region is obtained by multiplying the refrigerant density (which is easy to obtain in the thermodynamic tables) by the superheating region volume. Because the vapor density depends on the temperature, it is calculated using the average temperature $(T_{r1} + T_{r2})/2$. However, the refrigerant mass in the two-phase regions are more complicated because the refrigerant density varies significantly inside these components (in a non linear form). The density decreases when the fluid quality increases (the quality varies to values of approximately 20 % to 100 % in the evaporator). In general, a linear variation is a good representation of the quality change in terms of the tubing length. It is possible to find the actual profile of this variation in Feenstra et al. (78).

It is important to distinguish that while the quality could be considered linear the density could not be. Consequently, it is easy to understand that for the two-phase region (evaporation region at Fig. 14 is not feasible to use a similar method with only one control volume as done in the superheated region. Thus, to obtain accurate results using

the Otaki method, the evaporation region should be divided into N control volumes, and the density should be considered different in each one of these volumes.

Then, the mass in each control volume is calculated by finding the product of the two-phase local density (ρ_r) and the volume of the control volume (ΔV). Finally, the evaporation region mass is obtained using Eqs. 2.20 and 2.21.

$$M_{nb} = \sum^{N} \rho_r \, \Delta V, \tag{2.20}$$

and,

$$\rho_r = \rho_l \, (1 - \epsilon) + \epsilon \, \rho_v, \tag{2.21}$$

where ρ_l and ρ_v are the density of the saturated liquid and vapor, respectively, and ϵ is the void fraction, which can be better understood using Fig. 15. This figure shows a two-phase flow through a control volume and its cross-section, where A_v and A_l are the areas occupied by vapor and liquid phases, respectively (velocities u_v and u_l indicate that there is a liquid-vapor interface). The void fraction is defined as the ratio between the cross-sectional area occupied by vapor and the total area.

In the Otaki model, the void fraction was computed using Hughmark's correlation (7), which is a function of the vapor quality, saturation temperature and mass flow. Farzad and O'Neal (79) recorded several measurements and concluded that Hughmark's correlation appeared to provide the best results among the eight void fraction models that they compared. Poggi (72) indicates that Hughmark's correlation is preferred by researchers. Woldesemayat and Ghajar (80) and Winkler et al (81) show that Hughmark's correlation is still one of the most important correlations for void fraction determination. For example, Koury (82) developed a transient model for a refrigeration system consisting of a compressor with variable velocity, coaxial heat exchangers (water as secondary fluid) and an electronic expansion valve. The system was charged with 350 g of R-134a. Simulations were conducted to determine the variations in both the entrances and exits of the heat exchangers. The transient responses of pressure, temperature, mass flow and heat exchanger mass were successfully obtained through this model, which was used in conjunction with Hughmark's correlation to calculate the void fraction in the two-phase regions.

Hughmark's correlation for void fraction (ϵ) is given by Eqs. 2.22 and 2.23.

$$\epsilon_{hom} = \frac{1}{1 + \frac{\rho_v}{\rho_l} \, \frac{(1-x)}{x}}, \tag{2.22}$$

and,

$$\epsilon_{hug} = K \, \epsilon_{hom}. \tag{2.23}$$

Table A.2 – Factor K of Hughmark correlation as a function of the Z-parameter (7).

Z	1.3	1.5	2	3	4	5	6	7	10	15	20	40	70	130
K	0.185	0.225	0.325	0.49	0.605	0.675	0.72	0.767	0.78	0.808	0.83	0.88	0.93	0.98

The first expression is the void fraction given by a homogenous model in which the velocities u_v and u_l are assumed equal and x is the vapor quality. In the second expression, ϵ is the void fraction to be determined, ϵ_{hom} refers to the homogenous model for void fraction and the factor K is function of the empirical Z-parameter, given in Table A.2. The Z-parameter is calculated by Eq. 2.24.

$$Z = \left[\frac{d\,G}{\mu_l + \epsilon\,(\mu_l - \mu_v)}\right]^{1/6} \left\{\frac{1}{g\,d}\left[\frac{G\,x}{\rho_v\,\epsilon_{hom}(1-\epsilon_{hom})}\right]^2\right\}^{1.8}, \tag{2.24}$$

where d is the tube inner diameter, μ_l and μ_v are the dynamic viscosities of the liquid and vapor phases, respectively, G is the mass flux ($G = \dot{m}_r A^{-1}$, where $A = \pi d^2/4$), and g is the gravitational acceleration. The other terms of this equation were defined previously. Because the Z-parameter depends on the void fraction, it is necessary to use an iterative procedure to obtain the solution for Eq. 2.24. To perform these calculations, Otaki considered a linear profile for the quality along the heat exchanger.

Because this method is based on numerical methods and an iterative process, it can only be solved using computational resources.

Numerical experiments can complement the theoretical experiments because the simulations are able to evaluate millions of hypotheses over a very short time interval, until there is agreement with an expected result. However, the numerical model requires special attention to problems such as convergence of the results and sensitivity to entry data changes.

An alternative to the Hughmark's relation is the Rouhani's relation, modified by Steiner (83), which has a great acceptance, and this relation can be used as:

$$\epsilon_{rs} = \left\{\left[1 + 0.12(1-x)\right]\left(\frac{x}{\rho_v} + \frac{1-x}{\rho_l}\right) + \frac{1.18(1-x)[g\sigma(\rho_l - \rho_v)]^{0.25}}{G\rho_l}\right\}^{-1}. \tag{2.25}$$

As the above Eq. 2.25 does not depend on an iterative process, it is more stable and easier to use.

The procedure for calculating the refrigerant mass in a condenser is approximately the same as that used in the evaporator, except that the energy balance must be achieved not only in the superheated vapor region but also in the subcooling liquid. These balances lead to the determination of the one-phase region lengths. The condensation region length is obtained by subtracting the condenser total length from the one-phase regions

lengths. Thus, the refrigerant mass in the one-phase regions of the vapor and liquid are easily calculated, while the application of the void fraction model described previously allows determination of the charge in the condensation region. Besides, the quality varies between 100 % to zero.

To find the refrigerant mass in the compressor, Otaki considered the volume of this component and the average density of the vapor between the compressor suction and discharge. He applied a similar procedure to estimate the mass in the expansion device and in the liquid and vapor lines. Otaki calculated errors on the order of 10 % between the inventory estimation and the actual refrigerant charge. The tests were performed in seventeen machines equipped with tubular evaporators and condensers.

2.3.3 Modified Otaki method

Keep on the same example of the evaporator given in the section 2.3.2. The classical Otaki method as applied to an evaporator is essentially based on one equation and one unknown term. The equation is the energy balance in the one-phase (superheating) region and the unknown is the surface area (or length) of this region. Evidently, this energy balance must be characterized by temperature, pressure, mass flow, diameter and heat transfer coefficients. In general, these heat transfer coefficients are empirical, and they have an expected uncertainty. Particularly, certain air evaporators have unusual geometry thus making the heat transfer coefficient difficult to calculate with good accuracy. Therefore, the estimation of the refrigerant mass may be affected.

One way to improve this accuracy is to turn the problem into an algebraic system of two equations and two unknowns. One of unknowns remains the superheating region surface (S_{sh}), and the other unknown is the heat transfer coefficient on the secondary side ($h_s \cdot R_s$). Of course, a new unknown implies another equation (and another control volume). This second equation is obtained by applying the energy balance to the two-phase (evaporation) region, as described by Eqs. 2.26, 2.27, 2.28 and 2.29.

$$Q_{nb} = \dot{m}_r \, (i_{r3} - i_{r1}) = \dot{m}_s \, cp_s \, (T_{s3} - T_{s2}), \tag{2.26}$$

and,

$$Q_{nb} = U_{nb} \, S_{nb} \, \Delta T_{nb}, \tag{2.27}$$

and,

$$U_{nb} = \left(\frac{1}{h_{nb}} + R_w + \frac{1}{h_s \, R_s} \right)^{-1}, \tag{2.28}$$

and,

$$\Delta T_{nb} = \frac{\left[(T_{s2} - T_{r1}) - (T_{s3} - T_{r1})\right]}{ln\left[\frac{T_{s2}-T_{r1}}{T_{s3}-T_{r1}}\right]}, \tag{2.29}$$

where Q_{nb} is the heat transfer rate from the secondary fluid to the refrigerant in the evaporation region, i_{r1} and i_{r3} are the refrigerant enthalpies and T_{s3} and T_{s2} are the secondary fluid temperature at the entrance and exit of these regions, respectively. S_{nb} and ΔT_{nb} are the heat transfer surface area and logarithmic mean temperature difference. U_{nb} is the global heat transfer coefficient, which depends on h_{nb} (boiling heat transfer coefficient), h_s, R_s and R_w. The variables not mentioned here were previously defined in the description of the classical Otaki method. It is important to observe that the term $h_s \cdot R_s$ is considered constant in the one-phase and two-phase regions, which makes this evaluation possible.

The surface S_{nb} is not an unknown in the problem because it can be written as the difference between the total surface and superheating surface. As previously mentioned, the unknowns are S_{sh} and h_s, and the equations of the algebraic system are the energy balances in the superheating and evaporation regions. Of course, the boiling heat transfer coefficient (h_{nb}) must be calculated, and its value can be determined by Eqs. 2.30 and 2.31:

$$h_{nb} = C \left(\frac{1}{\chi}\right)^{n} h_l, \tag{2.30}$$

and,

$$\chi = \left(\frac{1-x}{x}\right)^{0.825} \left(\frac{\rho_v}{\rho_l}\right)^{0.5} \left(\frac{\mu_v}{\mu_l}\right)^{0.125}. \tag{2.31}$$

This expression is the basic form of a classical correlation used to calculate the boiling heat transfer coefficient and was originally proposed by Addoms (84), and it makes part of the Strictly convective relations. The final results of the inventory estimation were not impacted by the error in this correlation (85). Factor C and the exponent n are values that depend on the flow: for horizontal flow, C = 3.4 and n = 0.45; for vertical flow, C = 3.0 and n = 0.67. Term χ is the Martinelli parameter, which depends on the vapor quality, densities (ρ_l and ρ_v) and dynamic viscosities (μ_l and μ_v) of the liquid and vapor phases.

In the literature, there are several correlations to calculate the coefficient of heat transfer in the two-phase flow, as Kandlikar, Gungor and Winterton, as shown by Jabardo et al. (86). In this present work Addoms' correlation is used by two reasons: it generates good results to evaporators applied to refrigeration and air-conditioning systems (87) and (82); In the references (88) and (85), the authors tested several correlations and

concluded that Addoms' correlation provides the best results when considering balance of energy in evaporators.

To apply the modified Otaki method in a condenser, the energy balance must be applied in the superheated vapor, sub-cooled liquid and condensation regions. To construct these balances, certain data must be known, such as diameters, temperatures, pressures and fluid mass flow, as well as the internal heat transfer coefficients of the refrigerant in the three regions mentioned. The unknowns in this problem are the surfaces of the one-phase flow regions and the secondary fluid heat transfer coefficient. The condensation region surface value is obtained by subtracting the total surface of the heat exchanger from that of the one-phase regions. Finally, the refrigerant masses in the three regions are calculated in a manner similar to the methodology applied to the evaporator (in section 2.3.2).

Figure 16 shows a conceptual map and a comparison between the Otaki and modified Otaki methodologies.

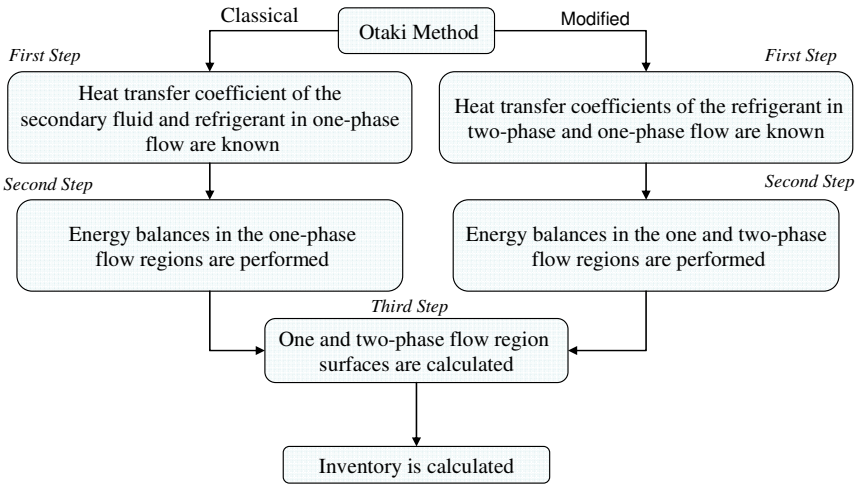

Figure 16 – Classical and modified Otaki method conceptual map.

Part III

Results

3 Results

3.1 Heat transfer validations

Heat transfer coefficient (HTC) for zeotropic mixtures as R-407C can be determined using the following methodology:

1. Select a general HTC relation for pure and azeotropic fluids;
2. Determine the reduction factor (K) to obtain an estimation of the nucleate boiling suppression for mixtures;
3. Multiply the nucleate boiling term by the reduction factor to obtain a corrected HTC for mixtures.

An important improvement on the results is reached once data for pure, azeotropic and zeotropic fluids are obtained under the same experimental conditions, and this fact generates a more reliable correlation. For example, all experimental data set is obtained from an oil-free experimental device (by using a micropump), using equivalent heat flux and evaporation temperature.

3.1.1 Correlation for pure and azeotropic fluids

Eq. 3.1 presents the relation obtained for pure and azeotropic fluids. This relation was obtained from 690 data points using the refrigerant fluids R-22, R-134a and R-404a. The methodology applied for obtaining this relation is presented in the Appendix 2.2.

$$
\begin{aligned}
h_{tp} &= (A_1 h_l^{1.713} + A_2 h_{nb}^{1.713})^{-1.713}, where,\\
A_1 &= a_0(a_1 \chi_{tt}^{b_1} + a_2(1 + 1.893\chi_{tt}^{-0.77})^{b_2} + a_3 Pr_{eq}^{b_3}) + c_0 Fr_l^{c_1}\left(\frac{\rho_{eq}}{\rho_{crit}}\right)^{c_2},\\
A_2 &= d_0\left[d_1\left(\frac{U_v}{i_{lv}}\right)^{e_1} + d_2\left(\frac{\rho_v}{\rho crit}\right)^{e_2} + d_3\left(\frac{\rho_{eq}}{\rho crit}\right)^{e_3} + d_4\epsilon^{e_4}\right] + f_0 Fr_l^{f_1} Pr_{eq}^{f_2}\epsilon^{f_3},\\
a &= [2.468, 0.156, 1.093, 0.756],\\
b &= [1.967, 0.230, 1.410],\\
c &= [-3.205, 0.887, 0.282],\\
d &= [1.248, 0.200, 8.925, -0.504, 0.468],\\
e &= [-0.485, 2.504, 0.484, -0.407],\\
f &= [-0.440, 3.923, 0.473, 16.827].
\end{aligned}
\tag{3.1}
$$

Eq. 3.1 is a semi-empirical relation, based on the Superposition Effects rule; term A1 is the enhancement factor and A2 is the suppression factor to the nucleate boiling. The results for the proposed general relation are presented in three scatter plots at Fig.17, Fig.18 and Fig.19 for the R-134a, R-404a and R-22, respectively; also, it is presented the results for Gungor and Winterton (4), Kandlikar (5) and Watellet (6).

It is possible to see by Figs.17, 18 and 19 that the relations tend to overestimate the experimental HTC, mainly for high values, and also a great improvement on the results, specially for the R-22, was achieved with the proposed relation.

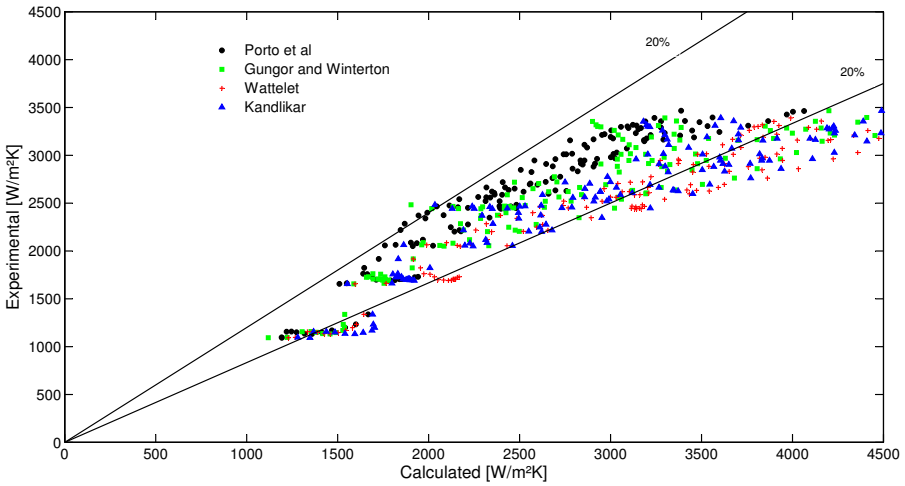

Figure 17 – Comparison between the general relation proposed for pure and azeotropic fluids (see Eq. 3.1), Gungor and Winterton (4), Kandlikar (5), Watellet (6) and the experimental data set for R134a.

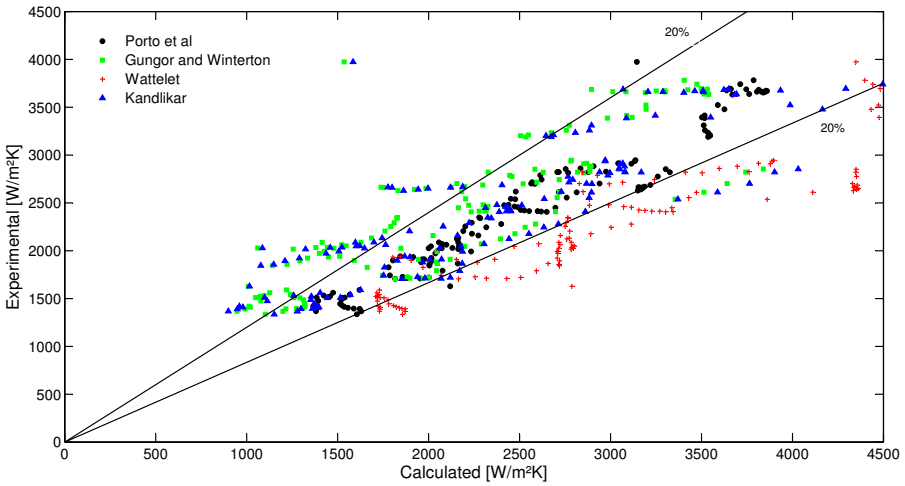

Figure 18 – Comparison between the general relation proposed for pure and azeotropic fluids (see Eq. 3.1), Gungor and Winterton (4), Kandlikar (5), Watellet (6) and the experimental data set for R404a.

Table A.3 presents the error metrics for the different relations tested, considering all fluids used. Looking at Table A.3 it is possible to notice that the proposed relation has a maximum mean absolute error below 10%, and the relations proposed by the other authors present a lower level of accuracy, specially for the R-404a, in which the mean absolute

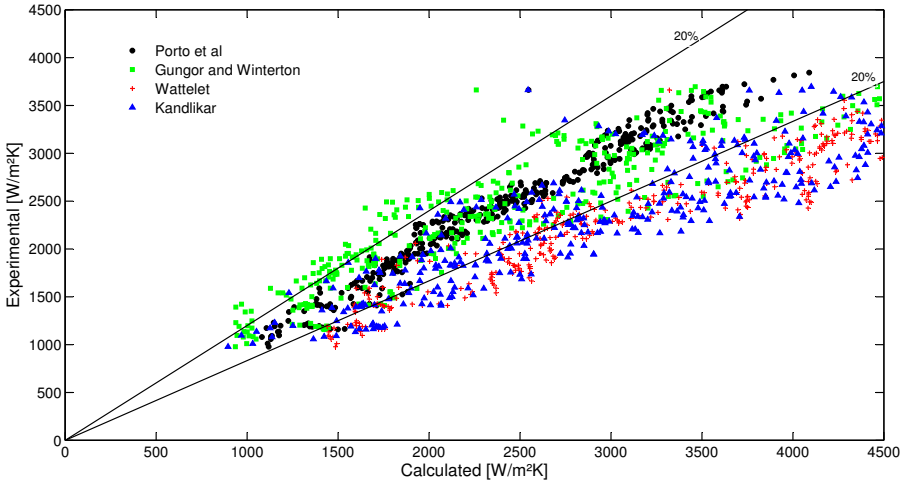

Figure 19 – Comparison between the general relation proposed for pure and azeotropic fluids (see Eq. 3.1), Gungor and Winterton (4), Kandlikar (5), Watellet (6) and the experimental data set for R22.

error is higher than 20% for Wattelet (6), Gungor and Winterton (4) and Kandlikar (5), and 7.71% for the proposed relation.

Also, it is important to prove that the proposed general relation presents good accuracy for all flow patterns. Fig. 20 presents the results for three different flow patterns inside the tube, indicating that the general proposed relation (HTC3) has a good performance for all different types of flow. The presented methodology is also compared in the Fig. 20 with an artificial neural network (HTC4b) and a strictly empirical relation (HTC1a), which uses the same data set and dimensionless parameters as HTC4b and HTC3, showing a very good accuracy even when compared with them. This comparison indicates that the proposed relation shows a high level of accuracy, regarding the optimized combination of dimensionless parameters, because the ANN has a much higher level of complexity than the relation proposed, but does not reflect this in better results. To facilitate using the proposed relation, Appendix A presents the Matlab function implemented for this new relation.

Table A.3 – Error metrics for the different general HTC relations, considering mean absolute percentage error (MAPE) and root mean square percentage error (RMSPE).

Refrigerant fluid		Porto et al. (Eq. 3.1)	Gungor/Winterton (4)	Wattelet (6)	Kandlikar (5)
R134a		7.54 (9.43)	11.13 (14.17)	18.47 (20.18)	15.2 (17.73)
R22	MAPE (RMSPE)	4.54 (6.4)	14.19 (17.2)	24.51 (25.6)	21.9 (24.4)
R404a		5.93 (7.71)	20.81 (28.73)	23.03 (24.67)	16.55 (25.92)

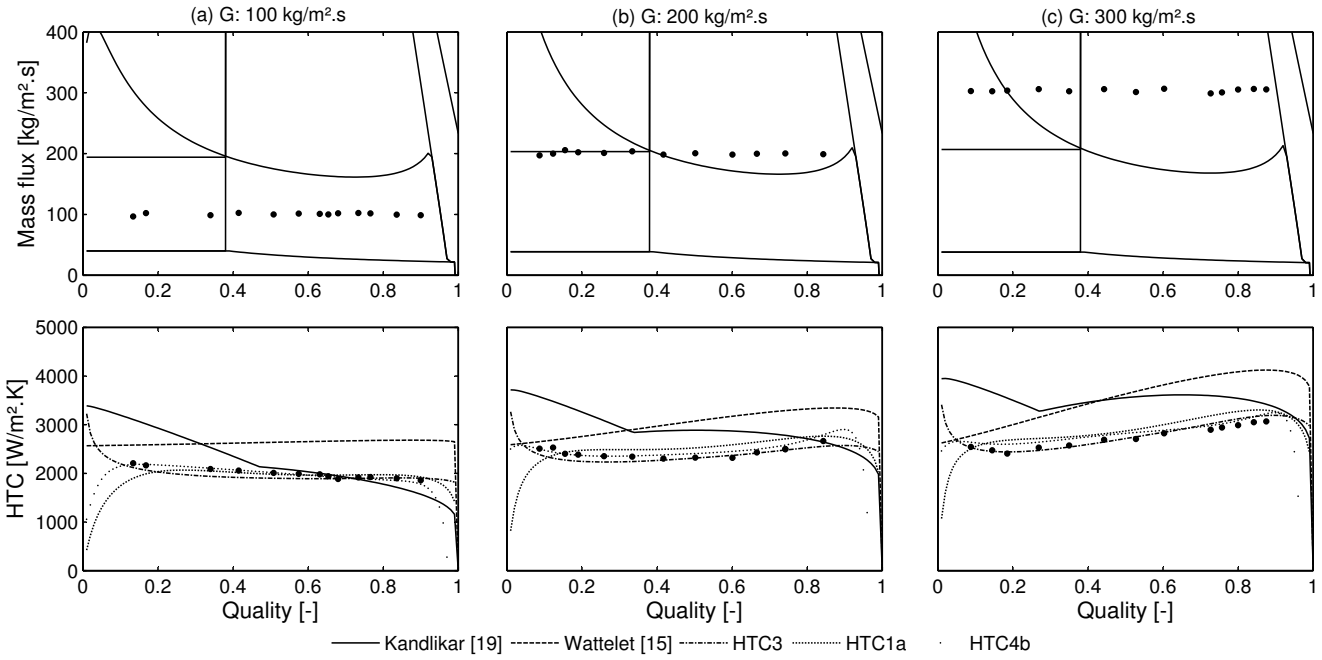

Figure 20 – Top: Flow pattern map and experimental points for the fluid R-22. Bottom: comparison between different methodologies for determining the HTC for R-22. HTC3 = Proposed relation; HTC1a = Strictly empirical relation; HTC4b = Artificial neural network relation.

3.1.2 Reduction factor for zeotropic fluids

Eq. 3.2 presents the relation proposed for the zeotropic mixture R-407C. The difference between Eq. 3.2 and Eq. 3.1 is the reduction factor for HTC nucleate boiling, K. The reduction factor used is the same as proposed by Thome (57), also including the fitting parameter B indicated by Gorenflo (56).

$$
\begin{aligned}
h_{tp} &= (A_1 h_l^{1.713} + A_2 \cdot K \cdot h_{nb}^{1.713})^{-1.713}, \\
&\quad and, \\
K &= \frac{h_{nb,p}}{\dot{Q}"} \Delta T_{bp} \left(1 - exp \frac{-\dot{Q}"}{\rho_l \, h_{lv} \beta / B}\right) = \\
&= \frac{h_{nb,p}}{\dot{Q}"} \Delta T_{bp} \left(1 - exp \frac{-\dot{Q}"}{\rho_l \, h_{lv} \beta / 1.15^{\Delta T_{bp}}}\right),
\end{aligned}
\tag{3.2}
$$

where β represents the mass transfer coefficient (estimated by Thome (57) as 0.0003 m/s), and B is the fitting factor estimated as the glide ΔT_{bp}; this approximation was made to express a direct relation between the glide and the resistance for mass transfer. Parameters A1 and A2 are the same as presented in Eq. 3.1.

Gungor-Winterton relation is also used in a modified version, as presented in

Eq.3.3.

$$h_{tp} = h_l \left[1 + 3000\ K\ Bo^{0.86} + 1.12\ K \left(\frac{x}{1-x} \right)^{0.75} \left(\frac{\rho_l}{\rho_v} \right)^{0.41} \right] \tag{3.3}$$

3.1.3 HTC validations

To validate the modified HTC for zeotropic fluids, Fig. 21, 22 and 23 present the results of an experimental validation for R-407C. Eq. 3.1 presents a good tendency but a deviation caused by the degradation on nucleate boiling; the reduction factor applied generated excellent results on the experimental points tested. Modified Gungor and Winterton relation (Eq. 3.3) also presented good results, specially for high quality.

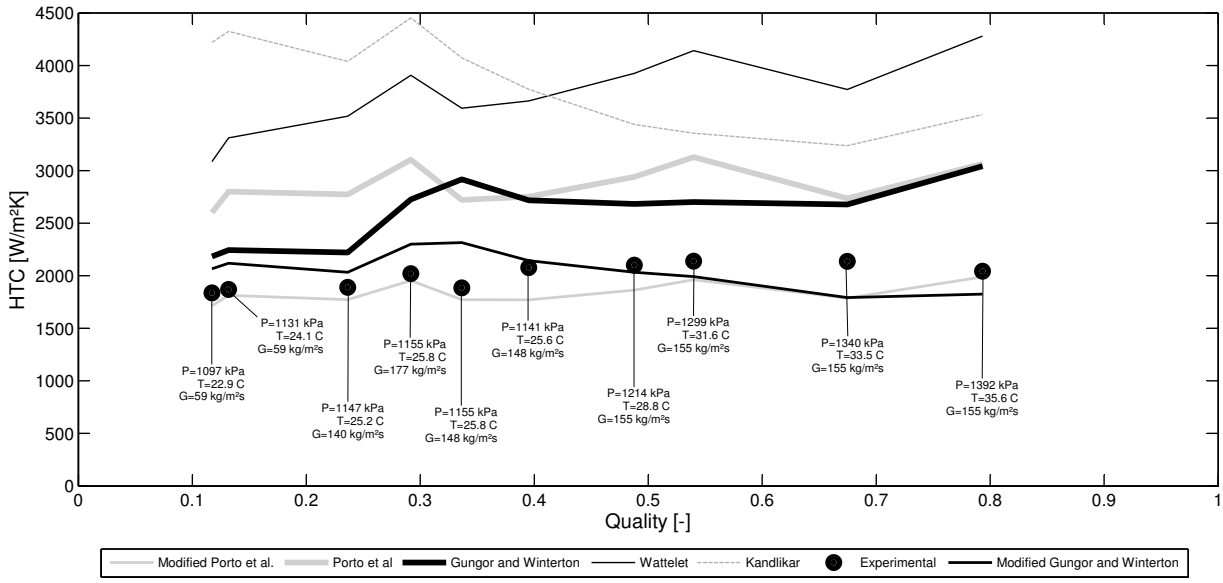

Figure 21 – First experimental validation of the proposed relation for pure fluids (Eq. 3.1), modified relation for mixtures (Eq. 3.2), applied to the refrigerant fluid R-407C at 12 kWm^{-2}; Porto et al. (Eq. 3.1), Gungor and Winterton (4), Kandlikar (5), Watellet (6) and Modified Gungor Winterton (Eq. 3.3) were also used to correlate the experimental data.

Fig. 23 shows that the modified Porto et al. relation underestimate the experimental values for high mass flow; high deviation is found for high quality, it is because Porto et al. relation is based on a data set which does not use quality over 80%.

3.2 Inventory validations

R-407C inventory study is accomplished in order to figure out which methodology presents the best results for the experimental device. Four different methodologies were applied on the data set, and the characteristics of each one are described below:

1. Inventory methodology: Otaki (74); void fraction model: Rouhani (47);

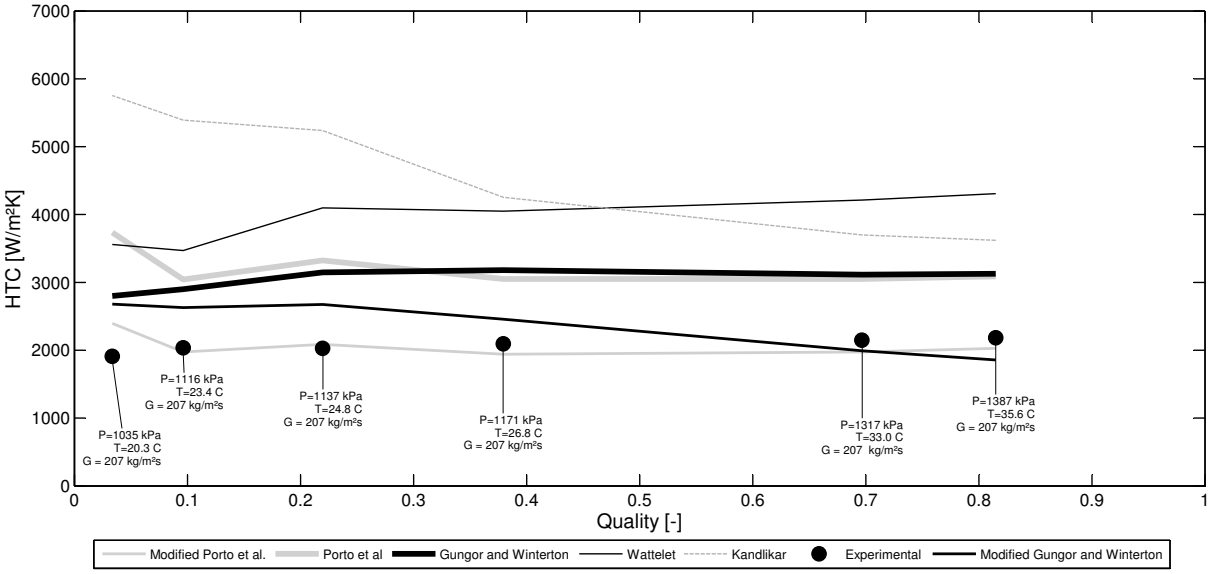

Figure 22 – Second experimental validation of the proposed relation for pure fluids (Eq. 3.1), modified relation for mixtures (Eq. 3.2), applied to the refrigerant fluid R-407C at $12kWm^{-2}$; Porto et al. (Eq. 3.1), Gungor and Winterton (4), Kandlikar (5), Watellet (6) and Modified Gungor Winterton (Eq. 3.3) were also used to correlate the experimental data.

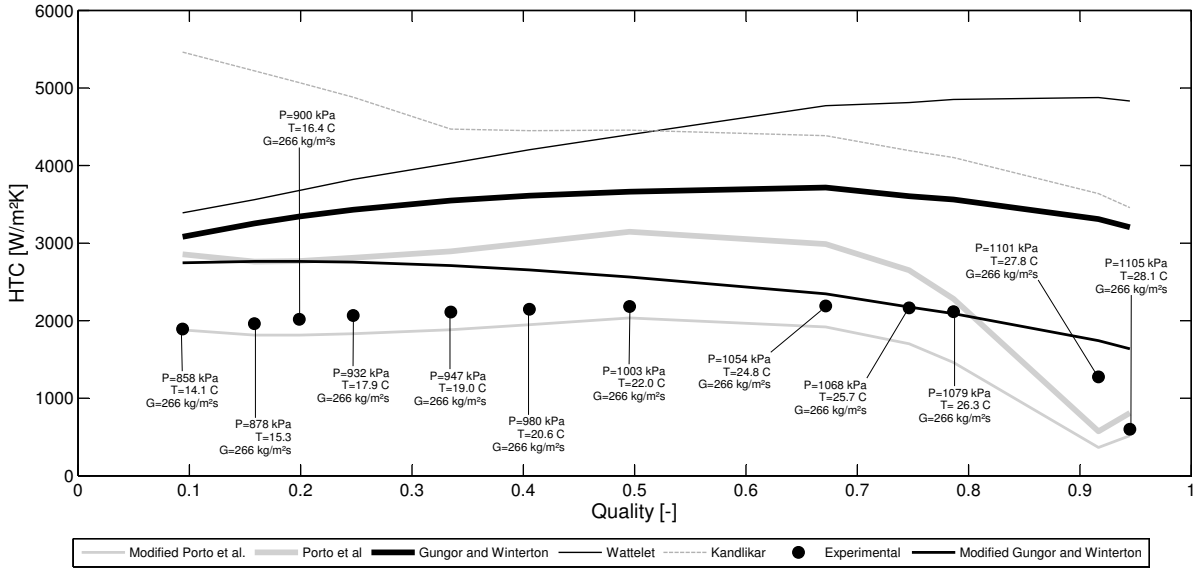

Figure 23 – Third experimental validation of the proposed relation for pure fluids (Porto et al., Eq. 3.1), modified relation for mixtures (Modified Porto et al., Eq. 3.2), applied to the refrigerant fluid R-407C at $12kWm^{-2}$; Gungor and Winterton (4), Kandlikar (5), Watellet (6) and Modified Gungor Winterton (Eq. 3.3) were also used to correlate the experimental data.

2. Inventory methodology: Otaki (74); void fraction model: Hughmark (7);

3. Inventory methodology: modified Otaki (77); void fraction model: Rouhani (47); two phase flow HTC relation: Shah (43);

4. Inventory methodology: modified Otaki (77); void fraction model: Hughmark (7); two phase flow HTC relation: Shah (43).

Figure 24, 25, 27 and 26 present simulations accomplished using the 4 methodologies presented above. All methodologies show a good accuracy, with small deviation from the estimated mass. The methodology "1", "2" and "4" have a good correlation, and "3" has the largest deviation.

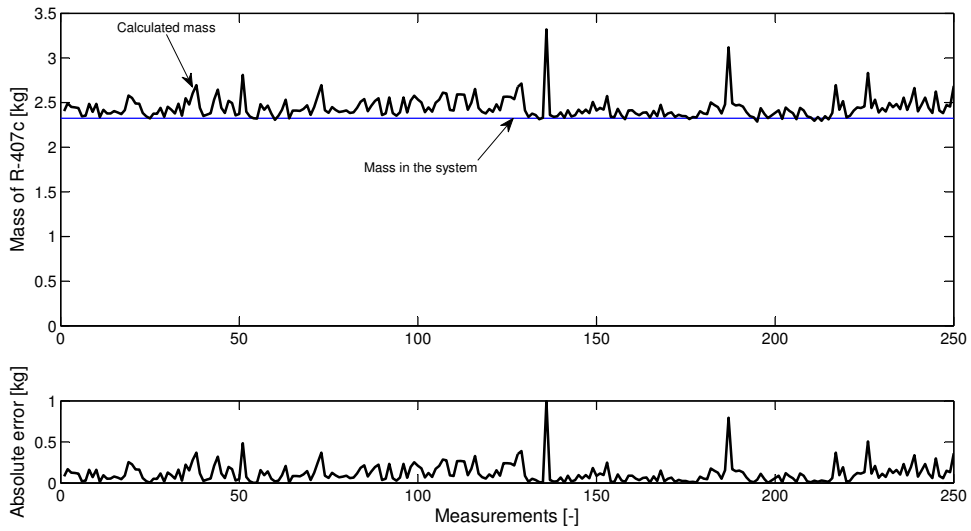

Figure 24 – Experimental results for using the methodology 1 (Otaki + Rouhani).

Comparing Rouhani and Hughmark, Rouhani's relation tends to overpredict the values of mass for the condenser; it occurs because Rouhani's relation tends to give lower values of void fraction, and the total mass increases, as can be seen in Eq. 2.21.

Comparing Fig. 24-25 with Fig. 26-27 is possible to see that the inventory calculated by modified Otaki tends to be higher than calculated by Otaki, and it occurs because the values of the overall HTC on the two-phase flow side tends to be overestimated in the condenser; when the overall HTC is higher than actual, the considered surface area occupied by two phase flow fluid is smaller, and the compressed liquid area is larger; as compressed liquid has a higher density, the calculated mass inside the condenser is higher than actual.

Error metrics are presented in Tab. A.4, indicating that all relations presented a smaller deviation than 10%, which is the expect deviation from the experimental values.

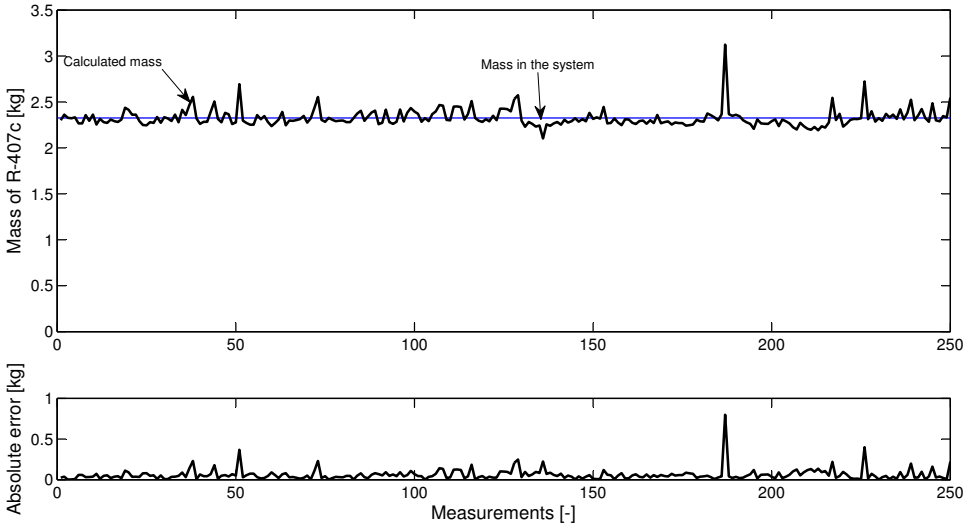

Figure 25 – Experimental results for using the methodology 2 (Otaki + Hughmark).

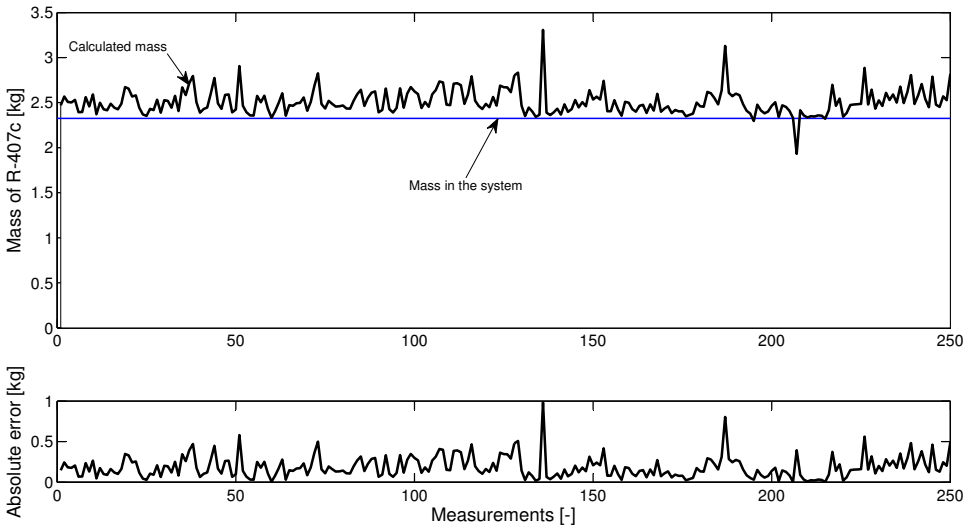

Figure 26 – Experimental results for using the methodology 3 (modified Otaki + Rouhani).

It is possible to conclude from these results that all methodologies are recommended to determine the inventory. Follow some additional comments:

- Methodology "1", "2", "3" and "4" are recommended to be used in all situations, generating accurate results;
- Methodology "2" and "4" are recommended in a situation on which the external coefficient of heat transfer is unknown, and it is difficult to be determined;
- Methodology "1" and "3" do not depend on iterative process, and because of this fact spends a lower computational time;

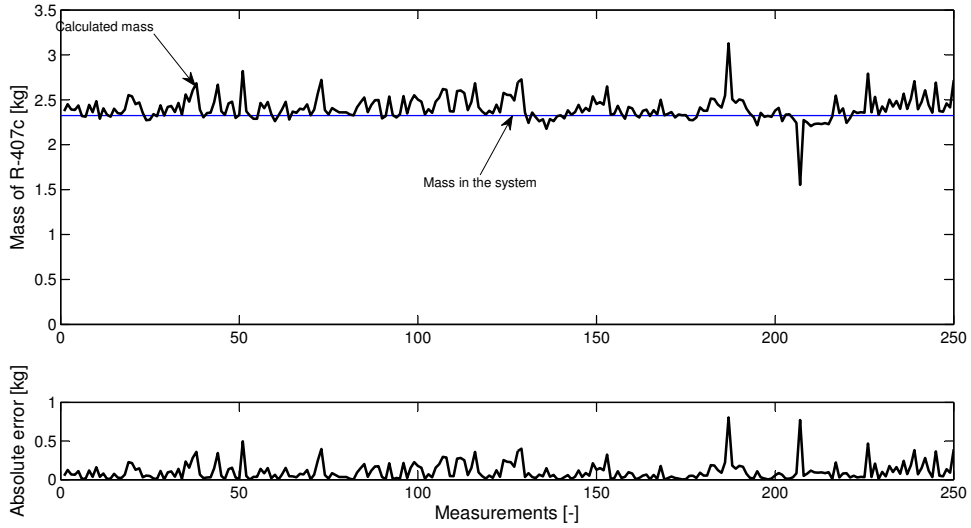

Figure 27 – Experimental results for using the methodology 4 (modified Otaki + Hughmark).

- Inventory validations were made considering the whole system contributions, and the contributions of each component in separate is not presented here; particularly on this tested device, the liquid line is proportionally larger than the vapor or two phase flow line, which determines a lower error metrics and a lower deviation between methods, as presented in Tab. A.4; it is expected during an experimental validation just on the condenser, for example, that the deviation among the relations be from 10 to 20%.

Table A.4 – Error metrics for the different methodologies to calculate the inventory, considering mean absolute percentage error (MAPE) and root mean square percentage error (RMSPE).

Methodology	1) Otaki + Rouhani	2) Otaki + Hughmark	3) modified Otaki + Rouhani	4) modified Otaki + Hughmark
MAPE	4.5843	2.557	7.1905	4.2119
RMSPE	6.0924	3.644	8.5703	6.3972

4 Conclusion

An experimental device was built to study the heat transfer and void fraction phenomena; this experimental device is comprised of four circuits working in parallel, allowing, *e.g.*, evaporation temperature change; a micropump was used to avoid oil contamination; electrical resistances were used as the heating device; the test section was validated using the energy balance on the pre-heater, and accurate results were found.

A general relation of HTC for pure and azeotropic fluids was obtained, using the methodology based on a semi-empirical relation combined with the Superposition Effects rule, and a large group of dimensionless numbers to comprise the suppression and enhancing factors; the relation proposed has a great correlation with the experimental data, and it is highly accurate, even when compared with artificial neural networks based relation; also, the relation presented high accuracy in all different flow patterns. Gungor and Winterton (1987) also presents a very good correlation, and this relation is highly recommended to be used combined with Thome's reduction factor relation for mixtures. This new relation has shown good accuracy during HTC validations for the R-407C, specially for quality lower than 80%, and it is because there were no experimental data over 80% to avoid axial conduction on the copper tube wall, which affects the uniform flux premise.

The HTC relation proposed is an empirical approach, and because of this fact is important as a future work improve the relation stability, in order to increase the reliability for a large range of experimental points.

Otaki and modified Otaki presented similar results during the inventory validations; Regarding the fluid R-407C, Otaki and modified Otaki were combined with Hughmark and Rouhani relation, presenting good results for all methods; modified Otaki tends to overpredict the inventory mass because of an overprediction on the overall heat transfer coefficient, but it is more recommended specially when the external surface area is complex and the external HTC is unknown.

As a future work is proposed studying the flow pattern map to improve the understanding on void fraction and HTC for the zeotropic mixture R-407C.

Bibliography

1 MAIA, A. *Metodologia de desenvolvimento de um algorítimo para o controle simultâneo da carga térmica e do grau de superaquecimento de um sistema de refrigeração*. Tese (Doutorado) — Departamento de Engenharia Mecânica, Universidade Federal de Minas Gerais, 2005.

2 LEE, J. et al. Experimental and numerical research on condenser performance for r-22 and r-407c refrigerants. *International Journal of Refrigeration*, v. 25, p. 3, 2002.

3 WANG, C.; HWANG, Y.; LIN, Y. Empirical correlations for heat transfer and flow friction characteristics of herringbone wavy fin-and-tube heat exchangers. *Int. J. Refrigeration*, v. 25, p. 673–680, 2002.

4 GUNGOR, K.; WINTERTON, R. A General Correlation for Flow Boiling in Tubes and Annuli. *Int. J. Heat Mass Transfer*, v. 29, p. 351 – 358, 1986.

5 KANDLIKAR, S. A general correlation for saturated two-phase flow boiling heat transfer inside horizontal and vertical tubes. *J. Heat Transf.*, v. 112, p. 219 – 228, 1990.

6 WATTELET, J. P. *Heat Transfer Flow Regimes of Refrigerants in a Horizontal Tube Evaporator*. Tese (Doutorado) — University of Illinois at Urbana Champaign, 1994.

7 HUGHMARK, G. A. An improved void fraction model for two-phase cross-flow in horizontal tube bundless. *Chem. Eng. Prog.*, v. 58, p. 62–65, 1962.

8 DEVOTTA, S.; PADALKAR, A. S.; SANE, N. K. Performance assessment of HCFC-22 window air conditioner retrofitted with R-407C. *Applied Thermal Engineering*, v. 25, p. 2937–2949, 2005.

9 HABERSCHILL, P. et al. Performance prediction of a refrigerating machine using R-407C: the effect of the circulating composition on system performance. *Int. J. Energy*, v. 26, p. 1295–1311, 2002.

10 CHEN, J.; KRUSE, H. Concentration shift simulation for the mixed refrigerants R-404A, R-32/R134a and R-407C in an air conditioning system. *HVAC & R Research*, v. 3, p. 149–157, 1997.

11 PASSOS, J. et al. Convective boiling of R-407c inside horizontal microfin and plain tubes. *Exp. Thermal Fluid Sci.*, v. 27, p. 705–713, 2003.

12 NECULA, H. et al. Simulation du functionnement d'un évaporateur à tubes et calandre utilisant le mélange zéotropique R-407c. *International Journal of refrigeration*, v. 24, p. 718–727, 2001.

13 WANG, C.; CHIANG, C. Two-phase heat transfer characteristics for R-22 / R-407c em um 6.5 mm smooth tube. *Int. J. Heat and Fluid flow*, v. 18, p. 550–558, 1997.

14 KEUMNAM, C.; TAE, S. Evaporation heat transfer for R-22 and R-407C refrigerant oil mixture in a micro fin tube with a U-bend. *International Journal of Refrigeration*, v. 23, p. 219–231, 2000.

15 JENG, Y.; CHANG, C.; WANG, C. Vapor pressure of R-410a/oil and R-407c/oil mixtures. *Applied thermal engineering*, v. 21, p. 863–870, 2000.

16 IDRISSI, M. Y. et al. Impact of refrigerant–oil solubility on an evaporator performances working with R-407C. *International Journal of Refrigeration*, v. 26, p. 284–292, 2003.

17 LIMA, C. *Convective boiling of refrigerants flowing in copper horizontal tubes*. Tese (Doutorado) — University of São Paulo, São Carlos School of Engineering, São Paulo, Brazil, 2000.

18 HAMBRAEUS, K. Heat Transfer coefficient of oil contaminated HCFC 134a in a horizontal evaporator. *Int. J. Refrigeration*, v. 18, p. 87–99, 1995.

19 PALM, B. *Heat transfer augumentation in flow boiling by aid of perforated metal foils*. Sweden: Royal Institute of technology. Dept. of Applied Thermodynamics and Refrigeration Stockholm, 1992. 87-99 p.

20 ANDERSON, S. W.; RICH, D. G.; GEARY, D. F. *Evaporation of R-22 in a Horizontal 3/4 in OD tube*. USA: ASHRAE Semiannual meeting – Houston, 1966.

21 MURATA, K.; HASHIZUME, K. Forced convective boiling of nonazeotropic refrigerant mixtures inside tubes. *J. Heat Trans.*, v. 115, p. 680–688, 1993.

22 JOHNSTON, J. R.; CHADDOCK, J. *Heat transfer and pressure drop of refrigerants evaporating in horizontal tubes*. USA: ASHRAE 71st annual meeting, Cleveland. Ohio, 1966.

23 WOJTAN, L.; URSENBACHER, T.; THOME, J. R. Investigation of flow boiling in horizontal tubes: Part I — A new diabatic two-phase flow pattern map. *Int. J. Heat Mass Transf.*, v. 48, p. 2955 – 2969, 2005.

24 KATTAN, N.; THOME, J.; FAVRAT, D. Flow boiling in horizontal tubes. Part 1: Development of a diabatic two phase flow pattern map. *J. Heat Transfer*, v. 120, p. 140–147, 1998.

25 KATTAN, N.; THOME, J.; FAVRAT, D. Flow boiling in horizontal tubes. Part 3: Development of a New Heat Transfer Model Based on Flow Pattern. *J. Heat Transfer*, v. 120, p. 156 – 165, 1998.

26 WOJTAN, L.; URSENBACHER, T.; THOME, J. R. Investigation of flow boiling in horizontal tubes: Part II — Development of a New Heat Transfer Model for Stratified-Wavy, Dryout And Mist Flow Regimes. *Int. J. Heat Mass Transf.*, v. 48, p. 2970 – 2985, 2005.

27 INC fChart S. EES: Engineering Equation Solver . 2012.

28 LATINI, G.; COCCI, G. R.; PASSERINI, G. *Transport properties of organic liquids*. England: Wit Press, 2006.

29 INCROPERA, F. et al. *Fundamentals of Heat and Mass Transfer*. Jefferson City: John Wiley Sons, 2007.

30 TAITEL, Y.; DUKLER, A. A model for predicting flow regime transitions in horizontal and near horizontal gas–liquid flow. *AIChE J.*, v. 22, p. 47 – 55, 1976.

31 ADDOMS, J.; DENGLER, C. Heat transfer mechanism for vaporization of water in a vertical tube. *Chem. Eng. Prog. Symp.*, v. 52, p. 95 – 103, 1956.

32 GUERRIERI, S.; TALTY, R. A study of heat transfer to organic liquids in a single tube, natural circulation, vertical tube boilers. *Chem Eng Prog Sym Series*, v. 56, p. 69 – 77, 1956.

33 CHADDOCK, J.; NOERAGER, J. Evaporation of R-12 in a horizontal tube with constant heat flux. *ASHRAE Transactions*, v. 72, p. 99 – 103, 1966.

34 CHADDOCK, J.; BUZZARD, G. Film Coefficients for in-tube evaporation of ammonia and R502 with and whitout small percentages of mineral oil. *ASHRAE Transactions*, v. 92, p. 22 – 40, 1986.

35 PANEK, J. *Evaporation Heat Transfer and Pressure Drop in Ozone-Safe Refrigerants and Refrigerant-Oil Mixtures*. Tese (Doutorado) — University of Illinois at Urbana-Champaign, 1992.

36 BANDARRA, F. *Study of Convective Boiling Heat Transfer of Halocarbon Refrigerants in Horizontal Tubes*. Dissertação (Mestrado) — Escola de Engenharia de São Carlos, Universidade de São Paulo, 1997.

37 DITTUS, F.; BOELTER, L. Heat transfer in automobile radiators of the tubular type. *University of California Publications in Engineering*, v. 2, p. 443 – 461, 1930.

38 CHEN, J. A correlation for boiling heat transfer to saturated fluids in convective flow. In: *6th National Heat Transfer Conference*. [S.l.: s.n.], 1963. p. 11 – 14.

39 GUNGOR, K.; WINTERTON, R. Simplified General Correlation for Saturated Flow Boiling and Comparison of Correlations to Data. *Chem. Eng. Res. Des.*, v. 65, p. 148 – 156, 1987.

40 JUNG., D.; RADERMACHER, R. Prediction of evaporation htc and pressure drop of refrigerant mixtures. *Int. J. Refrig.*, v. 16, p. 330 – 338, 1993.

41 LIU, Z.; WINTERTON, R. A general correlation for saturated and subcooled flow boiling in tubes and annuli, based on a nucleate pool boiling equation. *Int. J. Heat Mass Transf.*, v. 34, p. 1759 – 2766, 1991.

42 PIERRE, B. Coefficient of Heat Transfer for Boiling Freon-12 in Horizontal Tubes. *Heating and Air Treatment Engineer*, v. 19, p. 302 – 310, 1956.

43 SHAH, M. Chart Correlation for Saturated Boiling Heat Transfer: Equations and Further Study. *ASHRAE Transactions*, v. 88, p. 302 – 310, 1982.

44 GOSSELIN, L.; TYE-GINGRAS, M.; MATHIEU-POTVIN, F. Review of utilization of genetic algorithms in heat transfer problems. *Int. J. Heat Mass Transf.*, v. 52, p. 2169 – 2188, 2009.

45 MOHANRAJA, M.; JAYARAJ, S.; MURALEEDHARANB, C. Applications of artificial neural networks for refrigeration, air-conditioning and heat pump systems - A review. *Renewable and Sustainable Energy Rev.*, v. 16, p. 1340 – 1358, 2012.

46 BAKER, O. Design of pipe lines for simultaneous flow of oil and gas. *Oil Gas J.*, v. 53, p. 185 – 190, 1954.

47 STEINER, D. VDI-Wärmeatlas (VDI Heat Atlas). *Verein Deutscher Ingenieure, VDI-Gesellschaft Verfahrenstechnik und Chemieingenieurwesen (GCV), Düsseldorf*, 1993.

48 JABARDO, J.; BANDARRA, F. E. P.; LIMA, C. U. S. A new correlation for convective boiling of pure halocarbon refrigerants flowing in horizontal tubes. *Braz. J. Mech. Sci.*, v. 21, p. 245 – 258, 1999.

49 URSENBACHER, T.; WOJTAN, L.; THOME, J. Interfacial measurements in stratified types of flow. Part I: New optical measurement technique and dry angle measurements. *Int. J. Multiphase Flow*, v. 30, p. 107 – 124, 2004.

50 PICANçO, M. A. S.; BANDARRA, E. P. F.; PASSOS, J. C. Heat Transfer Coefficient Correlation For Convective Boiling Inside Plain And Microfin Tubes Using Genetic Algorithms. *Proceedings of the 11 th Brazilian Congress of Thermal Sciences and Engineering – ENCIT, Braz. Soc. of Mechanical Sciences and Engineering – ABCM, Brazil*, 2006.

51 COOPER, M. Saturated nucleate pool boiling: A simple correlation. *First UK Natl. Heat Transfer Conf.*, v. 2, p. 785 – 793, 1984.

52 FLETCHER, R. *Practical Methods of Optimization*. [S.l.]: John Wiley and Sons, 1987.

53 BISHOP, C. *Neural networks and their applications*. [S.l.: s.n.], 1994. 1803-1832 p.

54 HOLLAND, J. *Adaptation in natural and artificial systems*. [S.l.]: The University of Michigan Press, 1975.

55 VENTER, J. *The Experimental Determination of the Forced Convective Boiling Heat Transfer Coefficients of the Non-azeotropic Refrigerant Mixture R407C*. Tese (Doutorado) — Potchefstroom University for Christian Higher Education, 2000.

56 GORENFLO, D. State of the art in pool boiling heat transfer of new refrigerants. *International Journal of Refrigeration*, v. 24, p. 6 – 14, 2001.

57 THOME, J. R. Nucleate pool boiling of hydrocarbon mixtures on a gewa-tx tube. *Heat Transfer Eng.*, v. 1, p. 37 – 44, 1989.

58 FUJITA, Y.; TSUTSUI, M. Heat transfer in nucleate pool boiling of binary mixtures. *International Journal of Heat and Mass Transfer*, v. 37, p. 291–302, 1994.

59 STEPHAN, K. *Heat transfer in condensation and boiling*. Berlim: Springer, 1992.

60 CAREY, V. *Liquid-vapor phase-change phenomena: an introduction to the thermophysics of vaporization and condensation process in heat transfer equipment*. London: Taylor and Francis, 1956.

61 WIJK, V.; VOS, A. S.; STRALEN, S. J. D. V. Heat transfer to boiling binary liquid mixtures. *Chem. Eng. Sci.*, v. 5, p. 68–80, 1956.

62 BENJAMIM, R. J.; BALAKRISHNAN, A. R. nucleate boiling heat transfer of binary mixtures at low to moderate heat fluxes. *J. Heat Transfer*, v. 121, p. 365–374, 1999.

63 THOME, J. R. Prediction of binary mixture boiling heat transfer coefficients using only phase equilibrium data. *International Journal of Heat and Mass Transfer*, v. 26, p. 965–974, 1983.

64 TOLUBINSKIY, V. I.; OSTROVSKIY, Y. N. Mechanism of heat transfer in boiling of binary mixtures. *Heat Transfer Sov. Res.*, v. 1, p. 6–11, 1969.

65 THOME, J. R. Latent and sensible heat transfer rates in the boiling of binary mixtures. *J. Heat Transfer*, v. 104, p. 474–478, 1982.

66 CALUS, W. F.; RICE, P. Pool boiling-binary liquid mixtures. *Chem. Eng. Sci.*, v. 27, p. 1687–1697, 1972.

67 CALUS, W. F.; LEONIPOULOS, D. J. Pool boiling-binary liquid mixtures. *International Journal of heat and mass transfer*, v. 17, p. 249–256, 1973.

68 KANDLIKAR, S. G. Boiling heat transfer with binary mixtrures: part i - a theoretical model for pool boiling. *Journal of Heat Transfer*, v. 120, p. 380–387, 1998.

69 SCHLINDWEIN, A. R. et al. Nucleate boiling of fc-87/fc-72 zeotropic mixtures on a horizontal copper disc. *Heat Mass Transfer*, v. 45, p. 937–944, 2009.

70 BJöRN, P. Refrigeration systems with minimum charge of refrigerant. *Appl. Therm. Eng.*, v. 27, p. 1693–1701, 2007.

71 FARZAD, M.; O'NEAL, D. System performance characteristics of an air conditioner over a range of charging conditions. *Int. J. Refrigeration*, v. 14, p. 321–328, 1991.

72 POGGI, F. et al. Refrigerant charge in refrigerating systems and strategies of charge reduction. *Int. J. Refrigeration*, v. 31, p. 353–370, 2008.

73 DMITRIEV, V.; PISARENKO, V. Determination of optimum refrigerant charge for domestic refrigerator units. *Int. J. Refrigeration*, v. 7, p. 178–180, 1984.

74 OTAKI, T. Holding refrigerant in refrigeration unit . In: *Proceedings of the 13 International Congress of Refrigeration*. [S.l.: s.n.], 1984. p. 535–544.

75 ZUKAUSKAS, A. Heat transfer from tubes in mass flow. *Adv. Heat Trans.*, v. 8, p. 93–160, 1972.

76 SPARROW, E.; ABRAHAM, J.; TONG, J. Archival correlations for average heat transfer coefficients for non-circular and circular cylinders and for spheres in cross flow. *Int. J. Heat Mass Trans.*, v. 47, p. 5285–5296, 2004.

77 PORTO, M. P.; KOURY, R. N. N.; MACHADO, L. An alternative method to estimate refrigeration system inventory. *Applied Thermal Engineering*, v. 52, n. 2, p. 313 – 320, 2013.

78 FEENSTRA, P.; WEAVER, D.; JUDD, R. An improved void fraction model for two-phase cross-flow in horizontal tube bundless. *Int. J. Multiphase Flow*, v. 26, p. 1851–1873, 2000.

79 FARZAD, M.; O'NEAL, D. L. The effect of void fraction model on estimation of air conditioner system performance variables under a range of refrigerant charging conditions. *Int. J. Refrigeration*, v. 17, p. 85–93, 1994.

80 WOLDESEMAYAT, M. A.; GHAJAR, A. Comparison of void fraction correlations for different flow patterns in horizontal and upward inclined pipes. *Int. J. Multiphase Flow*, v. 33, p. 347–370, 2007.

81 WINKLER, J.; KILLION, J.; GARIMELLA, S. Void Fraction for condensing refrigerant flow in small channels, Void fraction measurement and modelling. *Int. J. Refrigeration*, v. 35, p. 246–262, 2011.

82 KOURY, R. N. N.; MACHADO, L.; ISMAIL, K. Numerical Simulation of a Variable Speed Refrigeration System. *Int. J. Refrigeration*, v. 24, p. 192–200, 2001.

83 WANG, H.; TOUBER, S. Heat Transfer to Boiling Saturated Liquids. *Verein Deutscher Ingenieure, VDI-Gessellschaft Verfahrenstechnik und Chemie-ingenieurwesen (GCV)*, 1993.

84 ADDOMS, J. N.; DENGLER, C. E. Heat transfer mechanism for vaporization of water in a vertical tube. *Chem. Eng. Prog. Symp.*, v. 52, p. 95–103, 1956.

85 MACHADO, L.; HABERSCHILL, P.; LALLEMAND, M. Refrigerant mass inside an evaporator in a steady or non-steady state. *Int. J. Refrigeration*, v. 21, p. 430–439, 1998.

86 JABARDO, J. M. S.; BANDARRA, F. E. P.; LIMA, C. U. S. A new correlation for convective boiling of pure halocarbon refrigerants flowing in horizontal tubes. *J. Mech. Sci.*, v. 21, p. 245–258, 1999.

87 WANG, H.; TOUBER, S. Distributed and non-steady-state modelling of an air cooler. *Int. J. Refrigrigeration*, v. 14, p. 98–110, 1991.

88 MACHADO, L. *Modele de simulation et étude expérimetale d'un évaporateur de machine frigorifique en régime transitoire*. Tese (Doutorado) — INSA de Lyon, 1996.

Appendix

APPENDIX A – Matlab function of the HTC proposed relation for pure fluids

%% Dimensionless parameters to be used in the function
a1(j,1)=1;
a1(j,2)=Rel;
$a1(j,3) = 1 + 1.893 * (Xtt)^{-}0.77$;
a1(j,4)=Frl;
a1(j,5)=Xtt;
a1(j,6)=rhol*Ul*d/mueq;
a1(j,7)=mueq * cpeq / keq*1000;
$a1(j,8) = hlv/Ul^2 * 1000$;
a1(j,9)=sigma/(Ul*mueq);
a1(j,10)=Uv/Ul;
a1(j,11)=rhol*Uv*d/mueq;
$a1(j,12) = d * 9.81/Ul^2$;
$a1(j,13) = d * (hlv * 1000)^{0.5} * rhol/mueq$;
$a1(j,14) = Ul/(hlv * 1000)^{0.5}$;
$a1(j,15) = sigma/((hlv * 1000)^{0.5} * mueq)$;
$a1(j,16) = Uv/(hlv * 1000)^{0.5}$;
$a1(j,17) = d * (hlv * 1000)^{0.5} * rhov/mueq$;
$a1(j,18) = d * 9.81/(hlv * 1000)$;
$a1(j,19) = P/Pcrit$;
$a1(j,20) = rhov/rhocrit$;
$a1(j,21) = rhoeq/rhocrit$;
$a1(j,22) = rhol/rhocrit$;
$a1(j,23) = T/Tcrit$;
$a1(j,24) = e1(j)$;
$a1(j,25) = xIA$;
$a1(j,26) = phi_cr * 1000$;
$a1(j,27) = Bo$;
$a3(j,1) = hl$;
$a3(j,2) = hnb$;
%% Dimensionless parameters to be used in the function

```
function h = correlation3(inputs,Hcnb)
x = inputs(:,2:end);
a = [2.4680 0.1560 1.9670 1.0930 0.2300 0.7560 1.4100 -3.2050...
0.8870 0.2820 1.2480 0.2000 -0.4850 8.9250 2.5040 -0.5040...
0.4840 0.4680 -0.4070 -0.4400 3.9230 0.4730 16.8270 1.7130];
iS1 = [2 4 6];
iS2 = [14 19 20 23];
iP1 = [3 20];
iP2 = [3 6 23];
xS1 = x(:,iS1);
xS2 = x(:,iS2);
xP1 = x(:,iP1);
xP2 = x(:,iP2);
nS1 = 2*size(xS1,2)+1;
nP1 = size(xP1,2)+1;
nS2 = 2*size(xS2,2)+1;
nP2 = size(xP2,2)+1;
aS1 = a(1:nS1); a(1:nS1) = [];
aP1 = a(1:nP1); a(1:nP1) = [];
aS2 = a(1:nS2); a(1:nS2) = [];
aP2 = a(1:nP2); a(1:nP2) = [];
yS1 = 0;
yP1 = 0;
yS2 = 0;
yP2 = 0;
if  isempty(xS1)
for i=1:size(xS1,2)
yS1 = yS1+aS1(2*i)*xS1(:,i).^  aS1(2*i+1);
end
yS1 = aS1(1)*yS1;
end
if  isempty(xP1)
yP1 = 1;
for i=1:size(xP1,2)
yP1 = yP1.*xP1(:,i).^  aP1(i+1);
end
yP1 = yP1*aP1(1);
end
y1 = (yS1+yP1).*(Hcnb(:,1).^  a(1));
```

```
if  isempty(xS2)
for i=1:size(xS2,2)
yS2 = yS2+aS2(2*i)*xS2(:,i).^  aS2(2*i+1);
end
yS2 = aS2(1)*yS2;
end
if  isempty(xP2)
yP2 = 1;
for i=1:size(xP2,2)
yP2 = yP2.*xP2(:,i).^  aP2(i+1);
end
yP2 = yP2*aP2(1);
end
y2 = (yS2+yP2).*(Hcnb(:,2).^  a(1));
Nu = (y1+y2).^  (1/a(1));
end
```